Evolution of the 2018 European heat wave

Stine Sagen

Thesis submitted for the degree of
Master of science in Meteorology and Oceanography
60 Credits

Department of Geosciences
Faculty of mathematics and natural sciences

UNIVERSITY OF OSLO

June 15, 2020

© 2020 Stine Sagen

Evolution of the 2018 European heat wave

This work is published digitally through DUO âĂŞ Digitale Utgivelser ved UiO
`http://www.duo.uio.no/`

Printed: Reprosentralen, University of Oslo

All rights reserved. No part of this publication may be reproduced or transmitted, in any form or by any means, without permission.

Abstract

This master study addresses the monthly evolution from April to September of the extreme heat wave that occurred in Europe in 2018. Heat waves cause serious hazards related to regional economics, ecosystems, human health and deaths. According to the large number of studies existing on heat waves, most climate models predict that in the future, heat waves will appear more often, last longer and increase in magnitude. Heat waves therefore require urgent attention and enhanced understanding of the processes behind this phenomenon is thus the motivation behind this thesis. The thesis will investigate how 1) atmospheric blocking was associated with a large-scale quasi-stationary mid-latitude flow regime and 2) soil moisture-temperature feedback could explain the anomalously high temperatures. To analyze these mechanisms and to see how they co-interact, a high resolution reanalysis dataset has been applied in order to provide a complete and consistent dataset. The main finding is that the strongest and most prolonged heat waves could mainly be identified in Northern Europe. In May, a strong heat wave which lasted between 12 to 36 days with a monthly mean temperature anomaly peak of approximately 6 °C could be identified in Southern Norway and Sweden. The exceptional temperatures could be explained from the high amount of days with a Scandinavian blocking regime which blocked the usual west to east traveling cyclones. As a result of the high frequency of atmospheric blocking, anomalously high positive downward radiative fluxes were identified over Southern Norway and Sweden which heated the surface and increased the latent heat flux, which contributed to soil drying and soil moisture was not found to control the latent heat flux. In June, the blocking from May was absent over Scandinavia, but a strong heat wave lasting for approximately 9 to 24 days over the British Isles was placed below an atmospheric blocking regime which could partly explain the prolonged heat wave. Nevertheless, the temperature anomalies were weak with a monthly mean temperature peak of approximately 3 °C. However, the soil moisture continued to decrease in Northern Europe which started to limit the latent heat flux and a significant soil moisture-temperature coupling could be recognized in Southern Sweden and a small part of Eastern Norway, but due to the absence of high pressure anomalies the daily mean temperature anomalies were quite weak. In July, a strong and long lasting heat wave again returned over Southern Norway and Sweden which lasted between 15-24 days with a monthly mean temperature peak of approximately 5 °C. The anomalously temperatures could be explained from an interlinkage between high anomalously frequency of Scandiavian blocking and soil moisture-temperature feedback which was reflected in the exceptional high negative latent heat flux anomalies of approximately $-20\frac{W}{m^2}$ and positive sensible heat flux anomalies of approximately $+40\frac{W}{m^2}$.

Acknowledgements

First of all I would like to thank my main supervisor, Jana Sillmann for providing me with help and support throughout the thesis. I will also like to thank my co-supervisor Frode Stordal for nice conversions and suggestions for the thesis. Both of you have provided me with a lot of motivation and positivity which have driven me through the year.

I will also like to thank all of my fellow students which I have been so lucky to get to know since I started my bachelor degree in Bergen some years ago, including the last couple of years at the master degree here in Oslo. It has been some fantastic years. The study has taught me a lot, and I'm very proud of myself of everything I have accomplished.

In the end I will also thank my family and my dear Sebastian for all their kindness and support through ups and downs.

Oslo June 15, 2020
Stine Sagen

Contents

1 Introduction

1.1 Motivation

Extreme weather and climate events consist of different types of severe weather related conditions covering a wide range of spatial and temporal scales. Such events occurring over a short time scale, usually below 10 days, are often noted as extreme weather events. Beyond these time scales, the events belong to climate extremes (Kirch et al., 2005). Heat waves are one type of extremes where the respective duration might range from few days and up to several weeks (which makes it both a weather and climate extreme phenomenon) often accompanied by serious drought conditions as a result of combined effects (e.g precipitation deficit and positive anomalously radiation).

In general, heat waves are a meteorological phenomenon characterized by an extended period of abnormally hot weather conditions, usually treated relatively to the normal weather in the area. However, at the present time no standard definition of a heat wave exists (Perkins and Alexander (2013); Habeeb et al. (2015)). Consequently, in defining a period as a heat wave event it's usually quite common to use different indices (see Theory Section 2.1).

Heat waves have gained large attention especially over recent years, both research related and by the general public as well. This is, in part, due to the increasing frequency of extreme heat wave events (Russo et al. (2015)) and the high impact of heat waves on many parts of the society. This includes serious hazards especially related to regional economics, ecosystems, human health and deaths (Meehl and Tebaldi, 2004). For instance, the 2003 European heat wave (mainly affecting Western Europe) is known for its extreme severity where additional deaths of about 70 000 people were estimated during that summer (Robine et al., 2008). The severity of heat waves might in general be caused by a single variable alone, e.g temperature. However, it's often arising from an interaction of several variables as well, in which not all necessarily serve as extreme. For instance high humidity in combination with hot days might increase the impact of

heat waves (Russo et al., 2017).

More recently, Europe experienced in 2018 several heat waves refereed to as the 2018 European heat wave that was a part of a broad heat wave striking the whole Northern Hemisphere. Northern Europe was especially affected due to unusual drought conditions present which led to water scarcity, crop failures and several wildfires (Skaland et al. (2019); Dirmeyer et al. (2020)). Figure 1.1 (a) below shows a satellite image over the North-Central European landscape during normally non heat wave conditions one year before 2018, whereas Figure 1.1 (b) shows how the land turned brown due to the dryness that occurred during the 2018 European heat wave. Southern Sweden, especially, experienced several wildfires (Dauphin and Stevens, 2018), highlighting the extremeness of this event. A literature review on this event is given in the Theory Section 2.5.

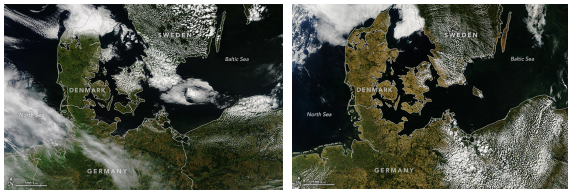

(a) July 19, 2017 **(b)** July 24, 2018

Figure 1.1: Satellite images captured by NASA's Terra satellite (a) North-Central European landscape conditions under 2017 compared to one year later (b) 2018 European Heat wave drought. Both Available from: `https://earthobservatory.nasa.gov/images/92490/heatwave-turns-europe-brown`, accessed: June 6, 2020.

Based on climate model simulations which examine future changes in heat waves, several studies show that in the future, heat waves will appear more often, last longer and increase in magnitude along with the increased temperatures related to global warming (Meehl and Tebaldi (2004); Collins et al. (2013)). The physical mechanisms driving heat waves need urgent attention in order to better understand how these interplay in generating extreme heat waves. Enhanced understanding of these processes will contribute to better representations of weather and climate extremes in climate models simulations (Sillmann et al., 2017) which serves as important for future adaption and mitigation due to the projected increases. Another important aspect is the rapid increase expected in the urban world population the coming years (Fent, 2008), which is likely to enhance mortality especially with respect to more frequent heat waves in a warming world (Jamei and Tapper, 2019). Investigating the 2018 European heatwave more closely is therefore of great relevance, and so will be the topic of this thesis. Before presenting the objectives and scope for the thesis, the following Section gives a brief introduction to some of the main

physical mechanisms typically involved in the onset and evolution of heat waves.

1.2 Heat waves and their driving mechanisms

Several studies on previous heat wave events in Europe, show that the development of summer heat waves in mid-latitudes (within the belt of westerlies) is mostly related to the large scale dynamics of different anomalously quasi stationary anticyclonic circulation patterns in the upper level flow, also known as blocking highs (Black et al. (2004); Matsueda (2011); Zschenderlein et al. (2018)). Such situations are associated with warm air advection and clear skies with an anomalous radiation budget bringing prolonged fair weather conditions at surface. However, usually the extreme temperatures and duration are not explained from the large scale dynamic circulation alone, but regional to local feedbacks (e.g feedbacks with soil moisture) are also important factors that amplify heat waves (Sillmann et al., 2017).

Thus, atmospheric blocking conditions might trigger regional soil moisture-temperature feedback interactions in which the impact of soil drying induces an increase in air temperature through a decrease in evapotranspiration/latent heat flux (see the Theory Section 2.3.4). Among others, Black et al. (2004) showed that the extreme temperatures during the 2003 European Heat wave were influenced by soil drying leading to a gradual increase in the sensible heat flux warming the near surface (see Theory Section 2.4). This in fact coincides with the findings from Miralles et al. (2014), but Miralles et al. (2014) concluded that temperatures in 2003 also escalated from the contribution of warm nocturnal residual layers mainly formed from enhanced convection during the daytime that re-entered the atmospheric boundary layer (ABL) over successive days.

In addition, positive anomalies in the sea surface temperature (SST) have also been found to be central drivers for certain heat waves. For instance, in a study on the 2003 European heat wave by Feudale and Shukla (2011), warm anomalies in SST in the northern Atlantic Ocean was shown to contribute to a northward shift of the jet stream revealing an expansion of the high pressure system over central parts of Europe affecting air temperatures.

1.3 Objective and scope

This master thesis has one main objective:

- Investigate the evolution of the 2018 European heat wave from the interlinkages between the mid-troposphere circulation and the soil moisture-temperature feedbacks.

We will further restrict the scope to a monthly evolution from April to September and focus on continental heat waves where all anomalies are obtained from using the 30 years reference period 1981-2010 as the climatology based on WMO (2019). Two different indices will be used in this thesis. The first index is a 2-dimensional blocking index called absolute geopotential height (AGP) adapted from Scherrer et al. (2006) with the aim of presenting the blocking frequency during the six months. The second is a heat wave index named HWMId (Russo et al., 2015) that aims to capture the spatial distribution of the strongest heat waves that occurred in 2018. In addition, the soil moisture-temperature feedback mechanism is explored through a correlation coefficient analysis. Based on these correlations, three regions are chosen to conduct regional averages of the monthly evolution in the heat budget (Figure 4.9 (a) shows the domains) to identify certain characteristics closer. To produce the analysis the atmospheric reanalysis data from ERA5 will be used and note that the thesis will treat each driver separately before Chapter 5 discusses the interlinkages of the mechanisms (see Chapter 5).

1.4 Outline

This master thesis consists in total of seven chapters. Each chapter's topics are listed below:

- **Chapter 1, Introduction:** The introduction gives a motivation and introduces some of the main mechanisms involved in heat waves followed by the objective and scope of the thesis and last raises the related research questions.
- **Chapter 2, Theory:** The theory chapter presents the necessary and relevant theoretical background and starts with the issue related to heat wave definition. Thereafter, high pressure and associated blocking phenomenon, soil moisture role in heat waves and the interplay among the mechanisms. Last, a brief literature study on the 2018 European heat wave is included.
- **Chapter 3, Data and methods:** The data and methods chapter begins by explaining the concept of reanalysis and provides information on ERA5 and the related data variables used. Then a description of the methods related to the two indices and the correlations are given in separately sections.

- **Chapter 4, Results:** The results chapter presents a description of the results.
- **Chapter 5, Discussion:** The discussion chapter discusses the results according to the objective of the thesis.
- **Chapter 6, Summary and conclusions:** The Summary and conclusions chapter provides a summary of main findings and presents conclusions.
- **Chapter 7, Limitations and future work:** The limitations and future work chapter presents the limitations for the thesis and give some brief successions for future work.

2 | Theory

This chapter begins with a discussion related to heatwave definitions based on indices and presents the particular definition used for this thesis. The relevant background theory related to large scale circulation and soil moisture are outlined in separately sections followed by the interaction among the two mechanisms in generating heatwaves. Last Section provides a literature study on the 2018 European heatwave.

2.1 Defining a heat wave event

Heatwaves are as already mentioned ambiguous which makes it difficult to come up with an universal definition. First, the temperatures experienced as unusual will of course vary relatively to the normal weather pattern in the area. Thus, heatwaves could be a particular season phenomenon or defined on an annual basis (Perkins and Alexander, 2013). Second, different additional constrains are involved in how various studies choose to define a heatwave. Mainly this include the choice of minimum length of consecutive days comprised of high temperatures, which type of temperature metric used (average, minimum or maximum), which aspects (e.g duration, magnitude and frequency), which approach (absolute vs relative temperature thresholds) and whether humidity is taken into account or not (Habeeb et al. (2015); Perkins and Alexander (2013)). Therefore, the choice of definition highly depends on the objective.

Several indices related to temperature extremes have been developed with the aim of providing useful aspects linked to the severity of heatwaves (Peterson et al., 2001). A range of different indices are discussed in for instance the literature study by Perkins and Alexander (2013). According to Perkins and Alexander (2013) certain weaknesses with the indices are present. One weakness it that many indices only consider one aspect of a heatwave, e.g it's duration only, frequency only or magnitude only. Especially one problem that might arise then is that two or more heatwaves consisting of different temperatures might be treated equally severe if the duration are the same (Russo et al., 2014). Another problem with the indices is that many of

them only apply to one group/area of interest in addition to a complex methodology that yields difficulties in comparing the severity of heatwaves in space and time.

Russo et al. (2014) introduce an index called Heat Wave Magnitude Index (HWMI) which is shown being capable of comparing heatwave magnitudes of different duration across time and regions. The HWMI merges duration and magnitude into one index number which defines the maximum magnitude of heatwaves in a year. The index estimates for every grid point a daily temperature threshold value for the 1981-2010 climatology. Based on this, a heatwave is defined as three or more consecutive days of maximum temperatures exceeding that threshold. According to the study by Russo et al. (2015), a weakness with the HWMI is that the indicator saturates at a certain level, e.g if the temperatures gets higher than the maximum of the reference period this might result in an underestimation of the respective magnitudes.

An improvement of the index called Heat Wave Magnitude Index daily (HWMId) is therefore used by Russo et al. (2015) to identify European heat waves, in which use a different procedure in attaining the index values. Specifically in that study, the index was used to rank the magnitude of the top ten European heat waves between 1950-2014 based on both daily maximum and minimum temperatures from observation data (E-OBS). The heat wave that occurred in Central Europe in 2003 have in several studies been considered very extreme (e.g Black et al. (2004); Black and Sutton (2007)) and the heat wave was captured by the HWMId as the second strongest heat wave. Figure 2.1 shows the map of HWMId based on daily maximum temperature (Tmax) in (a), corresponding heat wave duration in (b) and HWMId from daily minimum temperature (Tmin) in (c) for the 2003 European heat wave. A maximum local peak in the HWMId from Tmax can be spotted in Northwestern France (values between 36 to 48; brown color), but the HWMId general shows HWMId values from 15 to 36 over France with durations ranging from 9 to 15 days. HWMId from Tmin shows quite weaker values over a smaller area. However, the index confirms the severity of the heat wave of 2003 both from the daytime and nighttime aspect when compared to the index values from other heat waves (not shown here).

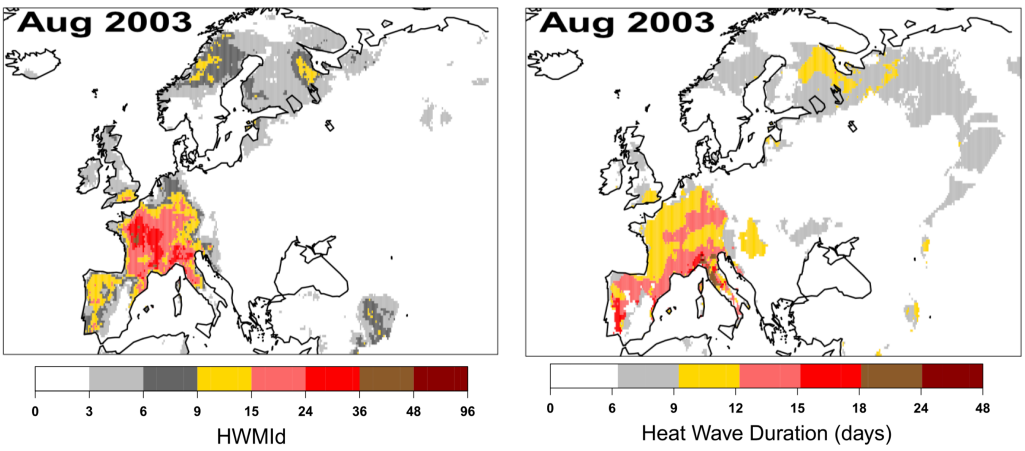

(a) (b)

Figure 2.1: HWMId based on Tmax (a) and corresponding duration (b) for the 2003 European heat wave (Russo et al., 2015)

Additionally the HWMId has also been used successfully to study heat waves for instance in Africa (Ceccherini et al., 2017) and for the 2016 European heat wave period (Zschenderlein et al., 2018).

As already mentioned in the first chapter (Section 1.3) HWMId will be the index used to define the maximum heat waves for the particular event of 2018, where a heat wave is defined as ≥ 3 consecutive days of maximum temperature above the threshold value between 1981-2010. The method of HWMId is described in more details in the Data and Method Chapter (Section 3.3).

2.2 Large-scale atmospheric circulation

2.2.1 Some basic dynamics involved in High pressure systems (anticyclones)

Since the air pressure for a given location at the Earth is a measure of the weight of the air above it, a high pressure system also referred to as an anticyclone is formed where the air above is denser compared relatively to the surrounding areas. An anticyclone is characterized by sinking air motions that is forced away (diverging) from it's pressure center near surface towards an area of lower pressure/cyclones (Allaby, 2020b).

Figure 2.2 shows an idealized anticyclone and the related dynamics involved (valid for North-

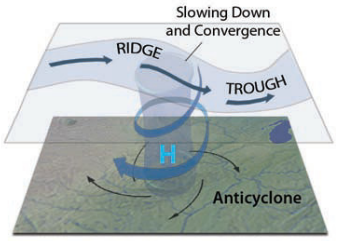

Figure 2.2: Anticyclone and the associated air flow In Northern Hemisphere extending from surface and to upper level flow near the altitude of the jet stream (Geography, n.d)

ern Hemisphere). Often, anticyclones at mid latitudes form as a result from convergence in Rossby waves (see the transparent belt with blue wind arrows aloft in Figure 2.2). Encyclopaedia Britannica (2020) defines Rossby waves as: "large horizontal atmospheric undulation that is associated with the polar-front jet stream and separates cold polar air from warm tropical air". Within the Rossby wave, the upper air flows from the wave ridge towards the wave trough in a west-east direction where the air slows and converges. As a consequence, the air sinks against the surface and warms adiabatic in which a high pressure area is found underneath the ridge to trough of a Rossby wave. Due to the rotation of the Earth (the coriolis force), the air around the pressure centre moves with a clockwise (anticyclonic) rotation parallel to the isohypses of constant geopotential height and near surface the air is diverging clockwise away with an angle to the isobars due to friction. The air from above replaces the loss of those air masses in order to achieve balance.

2.2.2 Impacts of anticyclones and links to heat waves

The warm and eventually dry air resulting from the adiabatic sinking may prevent rising moist air to cool and produce clouds. Therefore, high pressure systems in summer, normally brings fair weather associated with clear skies, lights winds and stable weather conditions at surface (Allaby, 2020b). Some Anticyclones appear as so called semi-permanent. These represents anticyclones in same locations over different years. However these semi-permanent anticyclones might weaken/strengthen or even extend meridionally. The "Azore High" semi-permanent pressure located in the North Atlantic Ocean approximately found at 30° N provides important influence on the weather in Europe, especially during summer due to its poleward extending (Allaby, 2020a). As mentioned in Chapter 1 (Section 1.2), heat waves usually develop with respect to a certain circulation feature known as blocking anticyclones/blocking highs which can be related to anticyclones persisting for several days.

2.2.3 What is atmospheric blocking?

According to Woollings et al. (2018), the word "blocking" in meteorology refers to a range of different large scale weather patterns in the middle to high latitudes where different interpretations exist in how to properly consider a blocking. However, often during an atmospheric blocking situation, the westerlies are disrupted and and meandering from its prevailing path for a longer period of time related to the Rossby waves. The Rossby waves might obtain a phase speed close to zero in which produce quasi stationary circulation patterns in which settle down the high pressures with characteristics similar to those mentioned in the Subsection above (2.2.2), but with possible higher impacts due to the long persistence. Thus, often a large anticyclonic anomaly can be seen in the blocked regions and the pattern blocks and steers the cyclones in other paths and thus is not uncommon to observe rainfall adjacent to the block. Examples of three common blocking types identified on a constant pressure surface at 500 hPa can be seen below:

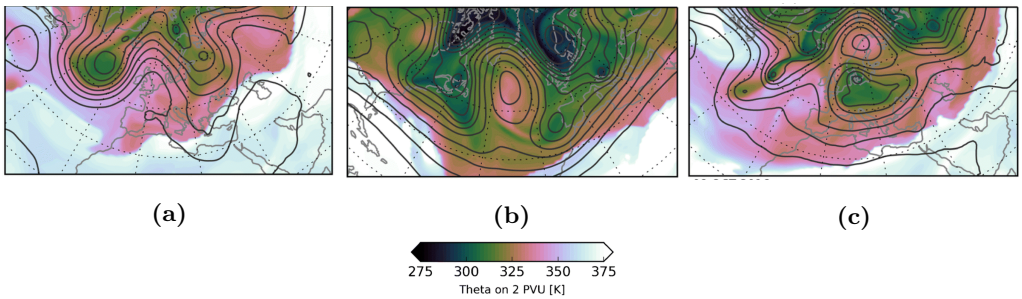

Figure 2.3: Snapshots illustrating different blocking types over the European Atlantic region. The contours are geopotential height at 500 hPa and the colors are potential temperature θ on the dynamical tropopause (PV = 2PVU) where (a) Summer ridge (08 Aug 2003), (b) Omega Block (25 Feb 2004) and (c) Rex/Dipole Block (09 Oct 2016). Adapted from Woollings et al. (2018)

Figure 2.3 (a) Demonstrates a typical "stationary (summer) ridge" associated with a large Rossby wave amplitude (large meandering of the westerlies). Figure 2.3 (b) shows quite similar pattern as the ridge in (a), but a larger amplitude and closed contours are present with more distinct troughs on both side of the ridge. Due to the shape nearly similar to the greek letter "Omega", the pattern is refereed to as "Omega block". A "dipole/rex block" (also sometimes refereed to as Scandiavian blocking) is seen in (c). This type of block is characterized by a large ridge with anticyclonic circulation to the north of a large trough with cyclonic circulation to the south. (Woollings et al. (2018)).

2.2.4 How to detect atmospheric blocking?

According to Doblas-Reyes et al. (2002), blocking is usually identified from two main different methods, either objective based or subjective based . The objective methods are based upon statistical approaches to obtain circulation patterns, whereas the subjective methods makes use of known synoptic scale features. The latter method often provides different indices used to detect blocking occurrence. This mainly includes indices based on lateral gradients in the upper level field where the geopotential height variable at 500 hPa (hereafter: Z500) are most commonly used. This include indices computed from absolute values or indices based on maximums in the anomalies of Z500 or potential vorticity (PV) as used by some studies (Schwierz et al. (2004); Scherrer et al. (2006)). However, to estimate blocking frequency in 2018 we restrict the chosen index for computations to the objective method and to the absolute Z500 field as well. In this thesis, as already mentioned we will use the index named "absolute geopotential height" (AGP) following the method in Scherrer et al. (2006). Scherrer et al. (2006) compared the AGP index to two other indices based on PV. From the climatology, they found based on the AGP index high values in the blocking frequency near the location of the Azore high outside of Southwest Europe (the Iberian Peninsula) in addition to smaller blocking frequencies over Europe compared to the two others. Thus, one weakness with the index is that the AGP index treat the strong semi-permanent anticyclone as a blocking phenomenon. The method is explained in Section 3.4 in the next Chapter.

2.3 Soil moisture

Soil moisture serves as an essential land surface variable included in land surface processes within the climate system for many reasons, but here we focus on its relevance with respect to particularly heat waves. Soil moisture directly impact the water and energy cycles through land evaportranspiration and the distribution of surface net radiation fluxes into the turbulent fluxes of sensible and latent heat. The respective sizes of these fluxes highly controls the transport of heat to or away from the surface and changes in soil moisture conditions might affecting the atmosphere through different feedbacks (Seneviratne et al. (2010); Dirmeyer (2011)). One of these feedbacks is the soil moisture influence on surface air temperature which will be explained in Subsection 2.3.4 later on. The following section provides a definition for soil moisture used in this thesis.

2.3.1 Definitions

There exist many definitions on soil moisture. Usually, the soil depth is divided into a saturated and an unsaturated zone in which soil moisture is related to the soil water being stored in the unsaturated soil zone, also called the vadose zone. Here we define soil moisture with respect to a given soil volume V, expressed as the volumetric soil moisture:

$$\theta = \left(\frac{\text{Volume of water in V}}{V} \right), \qquad [m^3_{H_2O}/m^3_{soil}] \tag{2.1}$$

The vadose zone is further subdivided into three more zones with respect to the water distribution: The root zone layer, the intermediate zone layer and the groundwater zone layer. The root zone layer is the upper most layer (approximately down to a 100 cm depth) and usually contains most of the plants roots that is supplied by water for plant transpiration demand. However, in this thesis we will only concentrate on the root zone layer, more precisely the surface layer down to 7 cm (see section 3.2.1). (Seneviratne et al., 2010)

2.3.2 Surface energy balance

Note that this and the following subsections are based on the paper by Seneviratne et al. (2010).

The soil is able to store large amounts of precipitation and energy and thus highly influence their respective surface budgets which is important for the land-atmosphere interactions. The evapotranspiration E includes bare soil evaporation and plant transpiration. However, hereafter we will mostly only consider E in form of latent heat flux which is converted by multiplying by λ denoted as latent heat of vaporization. A simple sketch of the energy budget of a surface soil layer is seen in Figure 2.4 and the corresponding equation can be written as:

$$\frac{dH}{dt} = R_n - \lambda E - SH - G \tag{2.2}$$

in which $\frac{dH}{dt}$ is the total energy change, R_n is net the surface net radiation, λE is the latent heat flux, SH is the sensible heat flux and G is the ground heat flux. We will omit the term G from Equation 2.2 when computing the components of the energy balance in this thesis, assuming it's small. The net radiation R_n at surface reads:

$$R_n = SW_{in} - SW_{out} + LW_{in} - LW_{out} \tag{2.3}$$

Where SW_{in} is the incoming short wave radiation reaching the surface, SW_{out} is the outgoing short wave radiation, LW_{in} is the incoming longwave radiation and LW_{out} is the outgoing longwave radiation (Seneviratne et al., 2010).

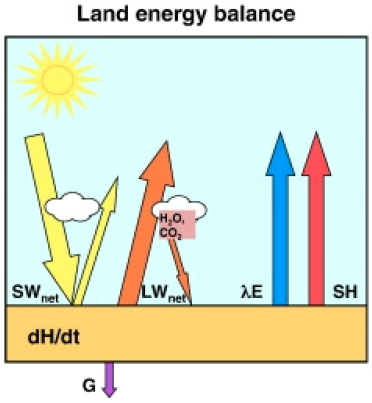

Figure 2.4: Surface energy balance. SW_{net} refers to the first two term in Equation 2.3, LW_{net} refers to the two second term in Equation 2.3 (Seneviratne et al., 2010)

2.3.3 Soil moisture-latent heat flux coupling

Figure 2.5 displays the coupling between the latent heat flux (evapotranspiration) regime against the soil moisture regime again based on the paper by (Seneviratne et al., 2010). The main purpose for showing this figure here and why it is of relevance is that there exist, according to classical hydrology, different regimes in which latent heat flux will reach a certain level when it is being controlled by the soil moisture which will have important implications for especially heat waves as will be explained soon. From the figure, there exist two main latent heat flux (evapotranspiration) regimes: a soil moisture limited regime (yellow color) and an energy limited regime (dark blue color). The energy limited latent heat flux regime consists of soil moisture values above some critical level (θ_{crit} in the figure). In this regime, the soil moisture does not controls the latent heat flux (or said in other words: latent heat flux is independent of the soil moisture). In the soil moisture limited regime, the soil moisture values are below θ_{crit}. In this regime, the soil moisture controls the latent heat flux (latent heat flux is dependent on the soil moisture). However, these two distinctions are not enough to decide weather latent heat flux is dependent or not dependent on soil moisture. Thus, soil moisture is further divided into three more regimes: a dry regime (orange color), the transitional regime (green color) and the wet regime (light blue color). Even though the soil moisture values are constrained to the soil moisture limited regime, a certain chance exist that the soil moisture might be too dry to constrain the variability of latent heat flux. In the latter case the soil moisture is confined to below the θ_{wilt}. In between the dry and wet soil moisture regimes, there exist a transitional regime in which soil moisture are most likely to control the latent heat flux. The major implication of this according to heat waves is that, when soil moisture is able to constrain latent heat flux more of the stored radiation can

be portioned into sensible heat flux and thus influence the air temperature. According to (e.g. Seneviratne et al. (2010); Dirmeyer et al. (2020), In Europe, a strong soil moisture-latent heat flux coupling is most likely to be seen in the areas close to the Mediterranean and less likely further north as e.g Northern Europe. The coupling addressed in this section leads further to the central concept of soil moisture-temperature feedback which is the second main mechanism after blocking of the thesis objective to explain temperatures under the 2018 European heat waves.

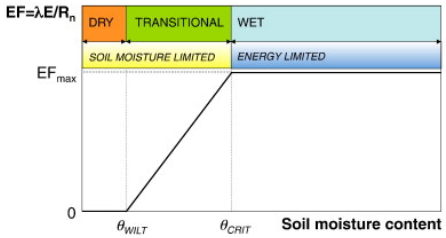

Figure 2.5: Soil moisture regimes and evapotranspiation regime (Seneviratne et al., 2010)

2.3.4 Soil moisture-temperature feedback

The major physical interactions involved in the soil moisture-temperature coupling and the subsequent feedbacks are displayed in Figure 2.6. The capital letters A, B and C indicate the associated steps where A: Dryer soil (negative anomalies) leads to a reduction in latent heat flux (evapotranspiration), B: More energy available for sensible heating in which increases the air temperature and C: Potential positive feedback that can lead to further increase in temperature which could be explained through: Higher temperatures can hold more water vapour, thus increasing the latent heat flux that possibly decrease the soil moisture even more in which can further enhance the temperature if the soil moisture, given the necessary soil moisture conditions are present (Seneviratne et al., 2010).

According to Dirmeyer (2011), land-atmosphere couplings can be divided into two segments: A terrestrial segment and an atmospheric segment. The terrestrial segment is directly connected to the soil moisture-latent heat flux coupling (A) in Figure 2.6 in which the radiative energy is not the controlling factor. The atmospheric segment is directly related to the linkage between the fluxes and the atmosphere (the temperature) (B) in Figure 2.6.

In this thesis I will therefore correlate soil moisture with latent heat flux (terrestrial segment) and correlate latent heat flux with the surface temperature (atmospheric segment). See Data and method chapter 3.5.1 for further explanations.

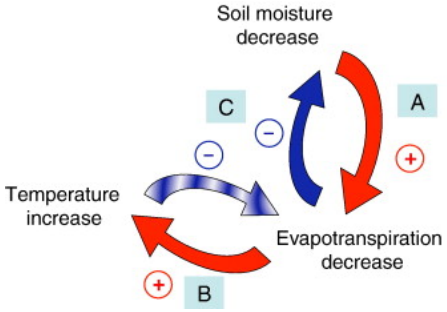

Figure 2.6: Soil moisture-temperature feedback loop. Red arrows represents couplings leading to drying/warming (positive feedbacks) and blue arrows represents potential negative feedbacks (Seneviratne et al., 2010)

2.4 Combined mechanisms in evolution of heat waves

The generation of extreme events arise usually from an interaction of several different components in the Earth system (Figure 2.7). This includes a combined convenient initial state with different drivers interacting with feedbacks and the presence of random processes. For heat waves particularly (red curve in Figure 2.7), an initial state of dry soil and for instance a later presence of blocking (or other drivers as well) as time progress might combined amplify the temperatures through positive soil moisture- temperature feedbacks producing extreme heat waves (subsection 2.3.4). (Sillmann et al., 2017).

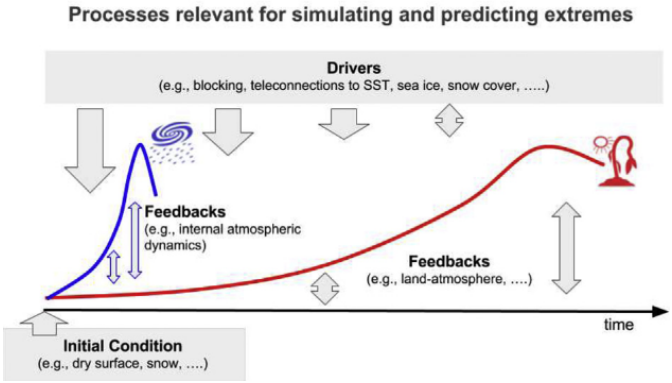

Figure 2.7: Sketch illustrating the generation of extreme events (Sillmann et al., 2017)

Figure 2.8 shows monthly area average evolution of turbulent and radiative fluxes including temperature anomalies over the summer of the 2003 European heat wave from a study done by (Black et al., 2004). This illustrates a typical heat budget characteristic seen during an evolution

of extreme heat wave event. Note that despite from being extreme, other heat wave events might show quite different characteristics due to for instance different duration, location, dataset used, climatology used etc. The temperature anomalies in 2003 peaked in June and August (Figure 2.8) (black and white hatced bar) and Black et al. (2004) showed that positive net radiative flux anomalies at the TOA (red bars) were seen throughout the months were associated with a persistent anticyclone in which increased the temperature in June. The anomalously net surface flux (purple bars) was approximately balanced with the turbulent flux (blue bar), but each component evolved in different directions after June. The latent heat flux (blue edge bar) became gradually negative associated with a decrease in soil moisture and more energy was available for sensible heating (orange edge bar), increasing the surface temperature in August.

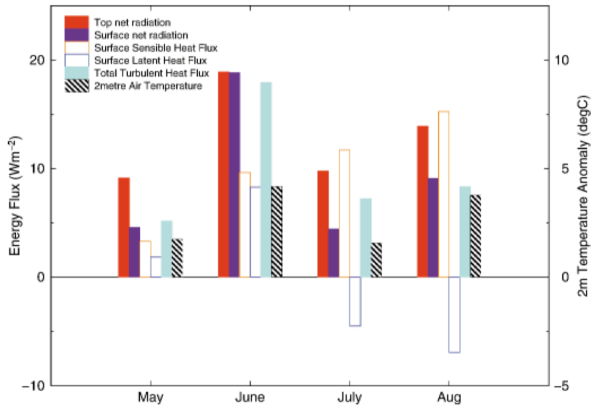

Figure 2.8: Energy budget of monthly anomalies averaged over the European land area ($0 - 20°$E, $42.5 - 52.5°$N), for May-August 2003. The data is from the ECMWF short-term forecasts (0-24 hours) as a deviation from the ERA-40 climatology for 1958-2002. The bars are anomalies in: TOA net radiative flux (red), surface net radiative flux (purple), surface sensible heat flux (orange edge), surface latent heat flux (blue edge) and surface turbulent flux (sensible heat flux + latent heat flux) (lightblue). Anomalies in 2 metre temperature (black and white hatched) are also seen. Radiative fluxes are defined positive downward, whereas turbulent fluxes are defined positive upward.

2.5 The 2018 European heat wave

During the year of 2018, European average positive anomalies relative to the 1981-2010 reference period were observed for all the months April to December (Climate Change Service, 2018). According to Climate Change Service (2018), long lasting positive temperature anomalies have been recognized in many months during the years of the 21st century indeed, but many have small magnitudes. However, The 2018 European heat wave stands as special compared to previous

ones due to its large extent and high long lasting temperatures (Skaland et al., 2019). Skaland et al. (2019) concluded that for Northern Europe, the unusual high temperatures and long lasting drought experienced in late spring and summer of 2018 could be explained from a weakened jet stream in which extended northwards providing a persistent anticyclone of continuously heating of the surface (associated with blocking).

The study by Dirmeyer et al. (2020) investigated the role of land-surface atmosphere interactions related related to the the soil moisture-temperature feedback mechanism under the 2018 European heat wave over the Northern Europe using combined reanalysis data from ERA5 and iu situ observations. Their results indicated a a positive feedback of a land-atmosphere interaction in which soil moisture limited the latent heat flux which heated the surface increasing the surface air temperature and reduced cloud cover despite its rare occurrence in these areas. (Seneviratne et al. (2010)) (see also Section 2.3.4).

3 | Data and methodology

The first part of this chapter provides information about the reanalysis dataset and the related variables used for conducting all the analysis in this thesis. Thereafter, we explain the steps involved in the calculations of the Heat Wave Magnitude Index Daily (HWMId), the atmospheric geopotential height (AGP) 2D-blocking index and the correlation analysis.

3.1 What is reanalysis?

The main purpose of creating reanalysis is to provide complete and consistent datasets that contains historical records of the atmosphere, ocean and land surface on a global scale. Reanalysis are being created from the concept of data assimilation where observations collected from different places on Earth and a numerical model are combined together into a complete covered dataset built on the laws of physics. The assimilation is based on the same methods used for the Numerical Weather Prediction (NWP). In the NWP, the initial conditions describing the state of the atmosphere at a particular time (the analysis) is estimated from combined previous forecasts and lately collected observations. However, the process in producing reanalysis operates on lower resolutions in order to achieve long records of data (Copernicus, 2018).

3.2 ERA5

ERA5 is a reanalysis dataset of climate data generated by the European Centre for Medium-Range Weather Forecasts (ECMWF) through one of their operative service called the the Copernicus Climate Change Service (C3S). The name ERA5 is shorthand for "ECMWF ReAnalysis", where the number 5 represents ECMWF's fifth main global reanalysis dataset which replace the previous one called ERA-Interim. The ERA5 dataset is available on a global scale ranging from the year of 1979 to present and as an improvement from the previous ERA-Interim reanalysis dataset, ERA5 contains variables at a hourly time resolution. The assimilation method used for this purpose is the four dimensional variational (4D-Var). The variables are created at model levels and at surface in addition to pressure levels, potential temperature levels and a potential

vorticity level. The resolution in horizontal is 0.25° x 0.25°. Whereas in the vertical, 137 model levels (hybrid sigma/pressure) are present with the top model level set at 0.01 hPa (Copernicus, 2018).

3.2.1 Data variables

The following variables from ERA5 (Copernicus, 2018) used in this thesis are listed below:

2m temperature, mean sea level pressure, convective rain rate, large scale rain rate, volumetric soil water layer 1 (0-7cm), surface latent heat flux, surface sensible heat flux, top net solar radiation, top net thermal radiation ,surface net solar radiation, Surface thermal radiation downwards (single levels) and Geopotential (pressure level at 500 hpa).

Vertical fluxes are defined positive downwards according to ECMWF. Note that, in this thesis the turbulent fluxes of latent and sensible heat flux are defined as positive upwards, wheras the radiative fluxes are unchanged.

3.3 Heat Wave Magnitude Index daily (HWMId)

HWMId has been defined in the Theory Section 2.1 and here we will present in more details how the method is implemented to obtain the index values. The procedure given here is mainly based on the study done for Europe (Russo et al., 2014) where 1981-2010 is used as the reference period. Note that the method is genesis based on maximum temperature (Tmax), but applies to minimum temperature (Tmin) and mean temperature (Tmean) as well.

The daily thresholds from the climatology 1981-2010 used to determine the presence of heat waves are computed from the 90th percentile of a set of data in each grid point containing daily Tmax, centered on a 31 day moving window given by:

$$A_d = \bigcup_{y=1981}^{2010} \bigcup_{i=d-15}^{d+15} T_{y,i} \tag{3.1}$$

in which $T_{y,i}$ is the daily maximum temperature in a year y for a given day i and $\bigcup$ represents an union of sets.

For a given year, the daily magnitude of each consecutive days in a heat wave period is computed as follows:

$$M_d(T_d) = \begin{cases} \frac{T_d - T_{30y25p}}{T_{30y75p} - T_{30y25p}} & \text{if } T_d > T_{30y25p} \\ 0 \text{ if } T_d \leq T_{30y25p} \end{cases} \tag{3.2}$$

where T_d is daily Tmax on day d contained in a heat wave period, T_{30y25p} and T_{30y75p} are the 25th and 75th percentiles of 30 years annual Tmax time series within the base period 1981-2010. As for the daily treshold, Equation 3.2 above is being calculated for each individual grid point.

The HWMId magnitude for a given heat wave period is attained by summing up the daily magnitudes for each day comprised in the heat wave period. The HWMId is then represented by the maximum value of the HWMId magnitudes that appears during a year. The daily heat wave magnitude unit of Equation 3.2 corresponds to the Inter quartile range (IQR) (difference between the 75 and 25 percentiles) of the 30 annual Tmax values. Therefore the temperature anomaly on a given heat wave day d with respect to 1981-2010 is given as the value of $M_d(T_d)$ times the IQR.

In this thesis the HWMId has been calculated by using the R package named "extRemes" which contains an implemented hwmid function (Gilleland, n.d).

In this thesis the following HWMId levels are defined:

- 0 - 3, 3 - 6, 6 - 9, 9 - 15, 15 - 21, 21 - 27, 27 - 30

When discussing the severity of the 2018 European heat wave 2018 according to this scale we will as mentioned use the HWMId computed for the 2003 European heat wave by Russo et al. (2015) as a comparable reference heat wave.

3.4 Absolute geopotential height (AGP) blocking index

To obtain a two dimensional map of estimated monthly frequency of blocking situations over the European Atlantic domain during the 2018 European heat wave, we use a absolute based blocking index named absolute geopotential height (AGP) adapted from the study by (Scherrer et al., 2006). The particular index consists of a 2-dimensional extension of the 1-dimensional blocking index presented by (Tibaldi and Molteni, 1990) (shortly: TM90 blocking index) in which variations in the geopotential height field at 500 hPa are examined. As done by Scherrer et al. (2006), the Z500 ERA5 data is interpolated into daily mean values on a 2.5 ° x 2.5 ° grid. The goal is to decide whether the grid points are considered "blocked" or "non-blocked".

First, gradients in the Z500 field are computed around some given central latitudes. The gradients are defined by Equation 3.3 and 3.4:

$$GHGS = \frac{Z(\phi_0) - Z(\phi_S)}{(\phi_0 - \phi_S)} \tag{3.3}$$

$$GHGN = \frac{Z(\phi_N) - Z(\phi_0)}{(\phi_N - \phi_0)} \tag{3.4}$$

Here, Z is geopotential height represented as a function of three latitude positions ϕ_N (the northern), ϕ_0 (the central) and ϕ_S (the southern).

To get an intuition of the idea, Figure 3.1 below shows a sketch. The two geopotential height gradients GHGN (Equation 3.4) and GHGS (Equation 3.3) are located roughly over and below the high pressure system denoted as the red H in the middle (center latitude: $\phi_M = \phi_0$) where the high pressure in this case reveals an area of high geopotential height values. Since the air flow is anticyclonic around high pressures, the westerlies lies to the north of the possibly blocking in the area of GHGN, while an easterly wind is seen to the south associated with the GHGS. Both gradients are estimated around all central latitudes ϕ_0 ranging from 35 °N to 75 °N (2.5 ° interval) in which the change between the central ϕ_0 and the southern ϕ_S (Equation 3.3) and ϕ_N and ϕ_0 (Equation 3.4) consist of a distance of 15°.

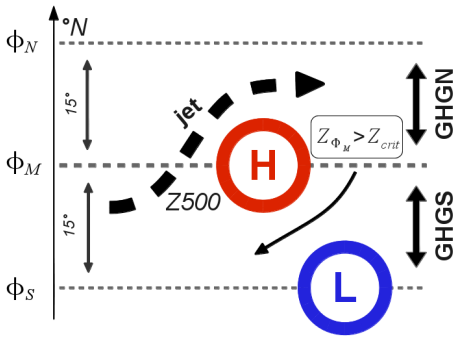

Figure 3.1: AGP blocking index illustration of a typical blocking situation (Richling, 2016).

From the idealised sketch, the jet stream (black hatched arrow) is separated into a northern stronger branch and a weaker southern branch connected to a geostropic circulation where the zonal component of the wind which consist of the meridional gradient of Z500 reads:

$$u_g = -\frac{g}{f}\frac{\partial Z}{\partial y} \tag{3.5}$$

Where Z is the geopotential height, g is the gravitaional acceleration and f is the coriolis parameter arising from the Earth's rotation.

The concept leads to the following two criteria:

1. GHGS $>$ 0,
2. GHGN $<$ -10 m/deg latitude

Where (1) is associated with the reversal of the westerlies in which u_g in Equation 3.5 is negative (easterly wind) due to a positive gradient in Z500. Opposite, (2) is related to a positive (westerlies) winds due to a negative gradient in Z500 where -10 m/deg latitude is approximately a geostrophic wind of 8 m/s. Thus in the case of (2) the westerly wind must exceed the defined threshold of at least 8 m/s in order to define a "blocking".

In addition to the two criteria (1) and (2) above, a third temporal criteria (3) exists which says that a given grid point is only blocked if persistence of at least 5 days are fulfilled. In this thesis the blocking frequency is presented as number of blocked days anomalies to the total days of the months treated separately with respect to the 1981-2010 average blocking frequency.

3.5 Linear relationships

To study the coupling between soil moisture and air temperature (the soil moisture-temperature feedback) we will perform a time correlation analysis of in total three sets of correlations to assess whether a linear relationship exist among the variables of interest. This include the relation of soil moisture to the surface fluxes (the terrestrial segment of the land-surface atmospheric response coupling) and the surface fluxes relation to the atmospheric response in air temperature near surface (the atmospheric segment of the land-surface atmospheric response coupling), see Theory Section 2.3.4 for details. In addition a correlation directly between the soil moisture and the surface air temperature as done in Gao et al. (2019) will be included in the analysis. The following subsection introducing the necessary approaches taken.

3.5.1 Calculating the correlation coefficient

Two main correlation coefficients approaches exist: The Pearson's correlation coefficient and the Spearman's rank correlation coefficient. Which one being the most appropriate one depends on the underlying distribution of the data. The Pearson correlation coefficient assumes that both variables are normal distributed due to its sensitivity to outliers in the dataset (data points differing significantly from the overall pattern in the dataset). Therefore, a non normal distribution pattern might provoke an overestimation/underestimation of the relationship. The Spearman's correlation coefficient is often more convenient when one or both data variables takes a skewed distribution (Mukaka, 2012).

We will use the Pearson's correlation coefficient to implement the needed relationships. Thus we need to assume that our data are being or at least approximately close to a normal distribution in every grid point. The sample Pearson correlation coefficient r is computed as:

$$r = \frac{\Sigma_{i=1}(x_i - \bar{x})(y_i - \bar{y})}{\sqrt{\Sigma_{i=1}^{n}(x_i - \bar{x})^2 \Sigma_{i=1}^{n}(y_i - \bar{y})^2}} \tag{3.6}$$

Where x_i and y_i denote each variable and the data points to be correlated and $\bar{x}$ and $\bar{y}$ are the sample means. The denominator represents the square root of the standard deviations of the two variables. The correlation coefficient r takes values on a scale from -1 (perfect negative association) to 1 (perfect positive association). In order to be consistent in the interpretation of the correlation coefficient we follow the suggested intervals and interpretations presented in (Mukaka, 2012) presented in Table 3.1 below.

Correlation	Interpretation
0.90 to 1.00 (-0.90 to -1.00)	Very high positive (negative) correlation
0.70 to 0.90 (-0.70 to -0.90)	High positive (negative) correlation
0.50 to 0.70 (-0.50 to -0.70)	Moderate positive (negative) correlation
0.30 to 0.50 (-0.30 to -0.50)	Low positive (negative) correlation
0.00 to 0.30 (0.00 to -0.30)	Negligible correlation

Table 3.1: Interpretation of correlation coefficient following Mukaka (2012)

In the correlations where soil moisture is used, the soil moisture feedbacks from the top most layer of the soil depth (0-7 cm) as done in for instance Gao et al. (2019) and (Dirmeyer, 2011) (note different depths depending on the data). This layer is picked because the surface layer provides the highest sensitivity to atmospheric forcings (Gao et al., 2019).

In summary, we compute the following correlations of daily mean values over monthly time periods:

1. r(SM,LHF)
2. r(LHF, T2m)
3. r(SM, T2m)

Where SM is short for soil moisture, LHF is short for latent heat flux and the T2m is short for the temperature at 2m. With respect to heat waves we expect to see a positive association of (1) and negative association of (2) in areas where soil moisture conditions plays an important role in influencing the air temperatures. As mentioned in the Theory 2.3.4, these relationships are often expected in areas of transitional wet-dry regimes. A negative correlation of (3) indicate a relationship between soil drying (or eventually opposite) and increase (decrease) in temperature, but the temperatures are not necessary a response of the soil drying itself. Consequently, to investigate a possible soil moisture-temperature coupling we should include the terrestrial segment (1) and the atmospheric segment (2) (Gao et al., 2019).

4 | Results

To explore the general evolution in the near surface monthly mean weather during April to September 2018, we first present the anomalies in terms of the meteorological parameters temperature, pressure and precipitation in addition to soil moisture due to their central role in heatwaves (see Theory Section 2.4). Afterwards we show the spatial distribution of the HWMId based on daily maximum and minimum temperature (associated with the night time temperature). Thereafter we showcase the monthly evolution in the blocking frequency anomalies estimated from the AGP blocking index before studying the soil moisture-temperature feedback by performing relevant correlations to diagnose the role of soil drying to a presence of positive temperature anomalies. The chapter ends with a monthly evolution of regional heat budget components over two chosen areas mainly based on the spatial distribution of the correlations. These regional analysis will be placed in context when discussing the bigger picture in how the 2018 European heatwave evolved in the next chapter.

4.1 Monthly evolution at surface

This section shows clear signs of evolution in heatwaves and drought affecting different places at varying magnitudes over the six considered months, mainly driven by the evolution of anomalously pressure conditions.

Monthly anomalies for 2018 in air temperature 2 metre above the surface are displayed in Figure 4.1. In April (4.1 (a)), positive temperature anomalies are seen throughout Europe where a large area of anomalously high temperatures ranging from 4 to 7 °C above the 1981-2010 average (see Appendix A 7.1 (a)) are centered over the Central, Eastern, Southeastern ans Southern Europe. In comparison, the anomalies are relatively weak (+1 to +3 °C) over remaining places in Europe. The location of extreme temperature anomalies are shifted towards the southern parts of Scandinavia and Finland in May (4.1 (b)). On the other hand, South-West Europe (Iberian Peninsula) and most parts of Iceland as well do show temperature anomalies of

-1 to -2 °C in this month. The temperature anomalies clearly weakens over most of the European countries in June (4.1 (c)). The Northern parts of Scandinavia are colder than average in June with anomalies of around -2 to -4 °C below the climatology (Appendix A 7.1 (c)). The Extreme temperatures from May return in July (4.1 (d)), but compared to May, the high temperatures are covering a larger area. However, the Western part of Iberian Peninsula are still reveled by colder than average temperatures. A shift in the temperature pattern is present in August (4.1 (e)) where many Northern countries show quite colder than average temperatures (approximately -1 to -2 °C). In the rest of Europe, the reanalysis yield positive deviations, now also including the Iberian Peninsula. Quite similar temperature patterns compared with August can be seen for September (4.1 (f)). However, a weakening in the anomalies over much of the Central Europe and an increase over the Iberian Peninsula with temperature anomalies of +2 to +3 °C.

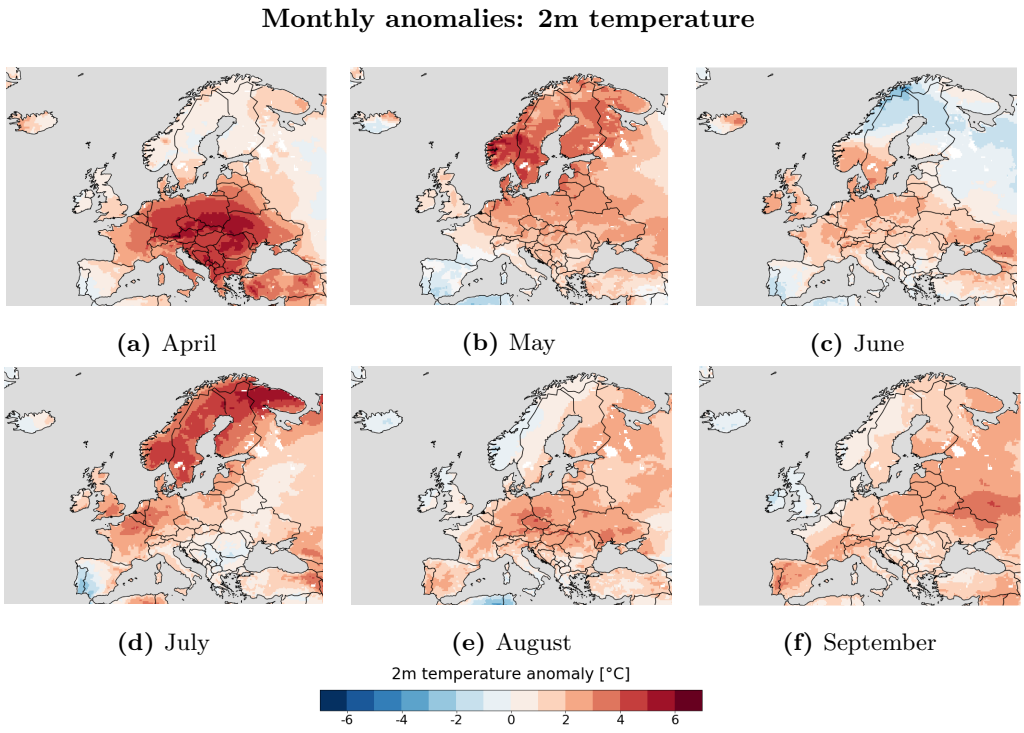

Figure 4.1: Anomalies in continental air temperature 2 metre above the surface relative to the reference period of 1981-2010 for the months April to September 2018. The red colors indicate temperatures higher than normal, whereas the blue colors are areas of colder than usual temperatures (unit: °C).

The extension of the semi-permanent Azores High pressure system located in the Atlantic Ocean basin South West of the Iberian Peninsula can be clearly identified from the climatology for all months (Appendix A 7.2), being strongest in July with a maximum pressure between 1023 hPa and 1025 hPa (7.2 (d)). An area of lower pressure (associated with the summer monsoon over Asia) is seen in the Eastern Mediterranean from June to July with a minimum pressure of 997 in July (7.2 (d)).

The monthly evolution in the corresponding anomalies for 2018 are presented in the Figure 4.2. From 4.2 (a), a distinct low pressure west of the British is seen in April (blue colors). Around the Southern Europe, positive pressure anomalies of approximately +2 to +4 hPa are present (orange colors). In May, the Azore High, west of the Iberain Peninsula in the Atlantic Ocean is stronger than usual (approximately maximum anomaly of +6 to +7 hPa) and are elongated with high pressure anomalies planted over the North Europe of approximately +8 to +9 hPa in the pressure centre over the Baltic sea areas (4.2 (b)). Positive pressure anomalies ranging from approximately +3 to +5 hPa are placed south of Iceland covering the British Isles in June (4.2 (c)). In July, high positive pressure anomalies are again appearing over the Nordic countries, but somewhat weaker compared to May (+6 to +7 hPa) where the pressure centre are found a little bit further north. The negative pressure anomalies seen over Southern Europe and Eastern Europe in June are extending further north in July (4.2 (d)). In August, the high pressure over the Northern Europe is replaced by a weak negative pressure anomalies having it's center in the Barents Sea, whereas a weak intensifying of the Azore High is recognized in the Atlantic Ocean in addition to positive anomalies over and near central Europe (4.2 (e)). The mean sea level pressure map for September then shows stronger positive anomalies of the Azore High south-west for the British Isles and the month is on average dominated by lower pressure over the Nordic areas (4.2 (f)).

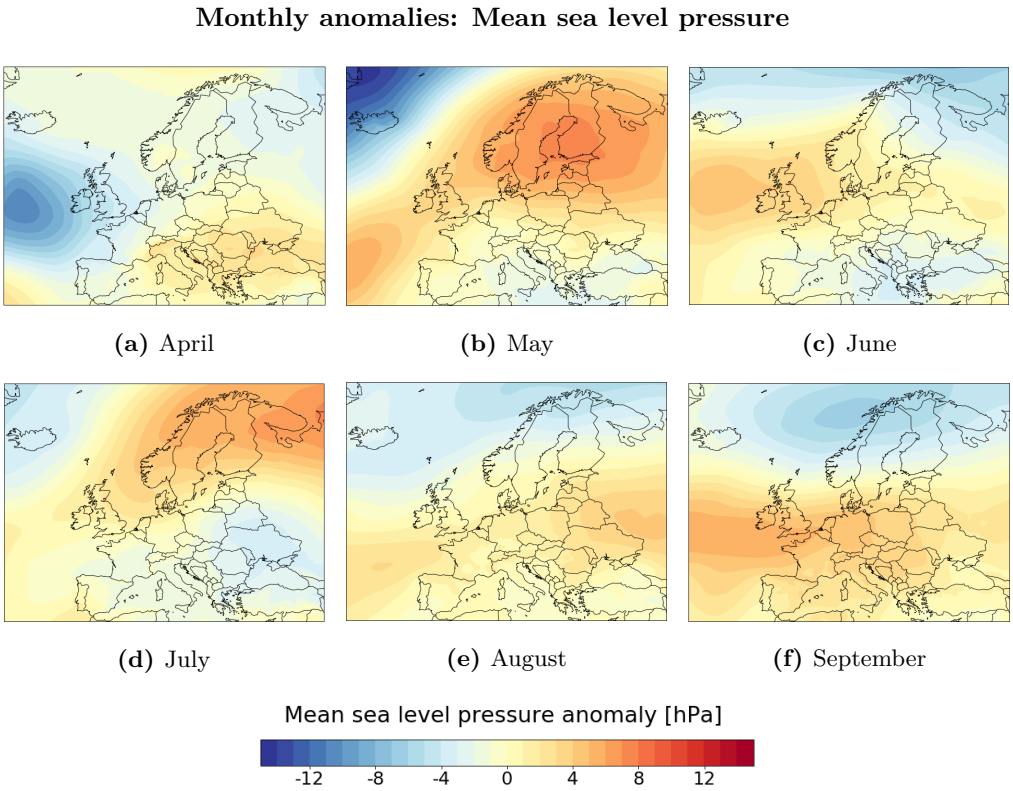

Figure 4.2: Anomalies in the mean sea level pressure relative to the reference period of 1981-2010 for the months April to September 2018. Orange-red colors indicate higher pressure than normal and the blue colors lower pressure than normal (unit: hPa)

Anomalies in the monthly amounts of total precipitation during 2018 are displayed in Figure 4.3 below. Southern Europe is dryer than usual in April with precipitation anomalies up to approximately -100 mm in some places. South-West Europe on the other hand is wetter in April with anomalies between +50 and +100 mm in North East Spain and Portugal (Appendix A (a) and 4.3 (a)). In May, the whole Southern Europe (including Northern Norway) is covered in positive precipitation anomalies where Italy and Western Turkey has the wettest weather of maximum anomalies reaching up to +200 mm (Appendix A (b) and 4.3 (b)). Positive anomalies in South Europe are also seen in June, but are extending a little bit further north covering some parts of East Central Europe as well. Finland is quite wetter than compared to it's climatology with anomalies up to +50 mm, also converging north for south Norway (4.3 (c)). Negative precipitation anomalies are dominating many parts of Northern Europe and Western Central Europe in July, while Eastern Central Europe and South East Europe have more precipitation than usual (4.3 (d)). More precipitation than normal are identified over most parts of Norway

in August (4.3 (e)), but the largest anomalies are along the west coast of Norway in September which shows up to +300 mm more precipitation (4.3 (f)). Central and Southern Europe are general dryer in September compared to the 1981-2010 climatology (approximately -50 to -100 mm), except from few places like for instance the East Coast of Spain, Austria and Scotland which have positive anomalies between 0 and 50 mm (Appendix A (e)).

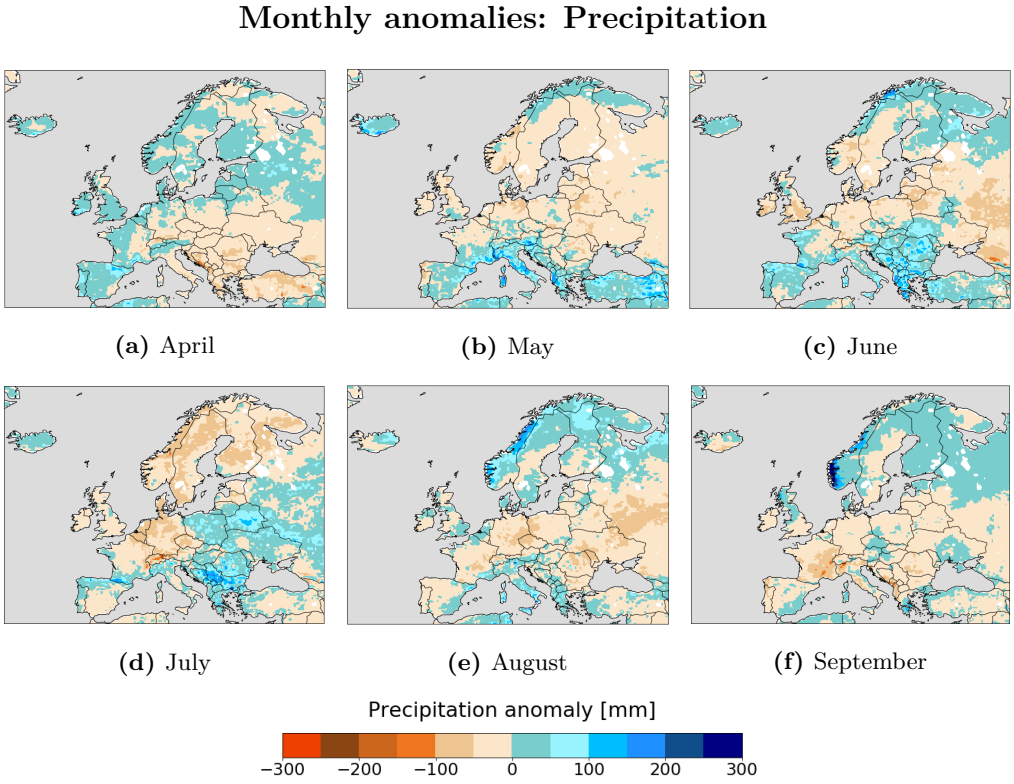

Figure 4.3: Anomalies in the monthly amount of total precipitation relative to the reference period of 1981-2010 for the months April to September 2018. Total precipitation is composed of a sum of convective and large scale precipitation. Blue colors show larger amounts of precipitation and red colors indicate less precipitation than usual (unit: mm)

.

Monthly deviations from climatology for the volumetric soil moisture content at a depth ranging from surface (0 cm) down to 7 cm, expressed as a percentage of soil water contained in that layer for each grid point, are seen in Figure 4.4 below. The climatology shows more or less constant soil moisture values from April to September (Appendix A Figure 7.4 (a)-(f)), with the driest soil found in the Southern Europe and South Western Europe decreasing from spring having approximately 20-30 % to the summer months values of approximately 10-20 % soil moisture content. The wettest soil is found in Finland (approximately 60-70 % water) where

Central Europe have more spread values ranging between 20-40 %.

In 2018, Eastern Central and South Europe do show negative anomalies in which the largest soil moisture anomalies are found in Eastern Turkey as high as approximately -20 % dryer in April. However, wetter than usual soil is dominating Spain and Portugal (approximately +5 to +7.5 %) (4.4 (a)) and rest of Europe are having soil moisture conditions close to the climatology deviating only slightly of approximately +5/-5 % (Appendix A). In the Northern half of Europe, the soil is more dry in May with anomalies between -5 and -10 % in Norway and Central Europe, while smaller positive anomalies are seen in for instance Sweden, Finland, Russia and Britain (< 5 %). In the Southern half of Europe, the soil is slightly wetter compared to climatology (between +5 to + 10 %) (4.4 (b)). June shows much of the same soil moisture pattern as May, but some stronger positive anomalies are seen in Southern Europe, especially North Spain and South Eastern Europe ((4.4 (c)). Figure 4.4 (d) for July clearly shows an intensified soil deficit over Southern Norway including Sweden, Denmark, the British Isles and north west central Europe with anomalies between approximately -5 to -15 %. In contrast, most other parts of Europe have soil anomalies of 0 to +15 %. In August, the anomalies over the Northern Europe have turned weakly (0 to +5 %) positive again, except from south Sweden, Finland and the southern part of the British Isles. Central Europe still have below average soil moisture content, which now also includes the areas east of Germany as well compared to July (Figure 4.4 (e)). September provides much of the same pattern seen in August, but the positive soil moisture anomalies also encloses southern Sweden and Finland (Figure 4.4 (e)).

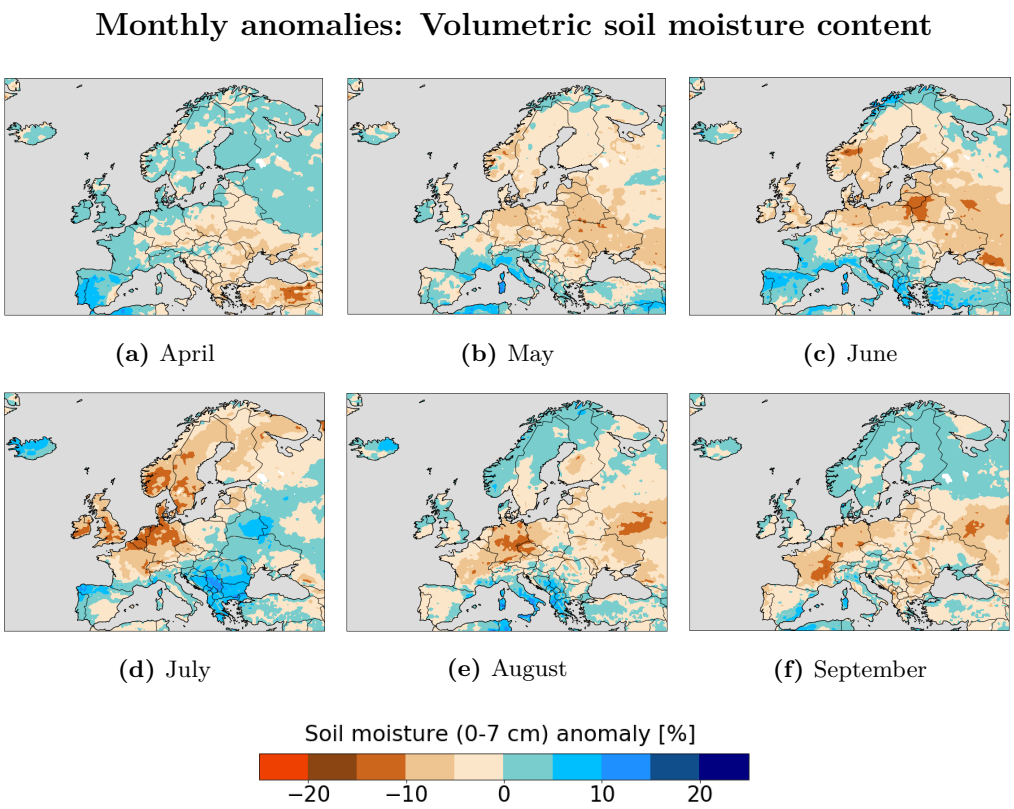

Figure 4.4: Anomalies in the volumetric soil moisture content at surface (0-7 cm) relative to the reference period 1981-2010 for the months April-September 2018. Blue colors indicate wetter than usual soil, whereas red colors dryer soil moisture content (unit: %)

4.2 Heat Wave Magnitude Index Daily (HWMId)

4.2.1 Daily maximum temperature (Tmax)

The spatial distribution of the maximum heat waves in 2018 based on daily maximum temperature (Tmax) and the corresponding duration are shown in Figure 4.5. It can be observed from Figure 4.5 (a) that nearly the entire European domain contains HWMId values > 3, except from some areas at Western part of Iceland and a small area in Southern Sweden with corresponding short duration below 6 days (Figure 4.5 (b)). The highest peak with HWMId values between 27 and 30 (brown color) are hardly recognized , but there exist a very small spot located in southern Norway surrounded by red color which is the second highest level of values defined in thesis to lay between 21 and 27. These values are identified in the southern part of Ireland, southern Norway, some locations in Eastern Norway and the along the east coast of southern Sweden. These areas show a heatwave duration between 18 and 36 days where the longest duration is seen in

the middle of southern Norway. The third largest HWMId level with values between 15 and 21 (pink color) are seen in middle and Eastern Norway having duration of 18 to 24 days, middle of Ireland and south west Britain, western Germany and some locations in Sweden and northern Russia where all heatwaves approximately last between 15 to 18 days. The middle level (gold color), defined here as HWMId values ranging from 9 to 15 are displayed in widespread parts of Europe, but mostly centered around Germany,Denmark, southern Norway and Finland, Britain ,Sweden and along the west coast of Italy. The associated duration (4.5 (b)) yield duration of 15 to 18 days for instance in southern Sweden and some shorter compared to for instance Germany (9 to 15). The dark grey colors representing HWMId values between 6 and 9 are dominating the northern parts of Norway, Sweden and Finland, Spain and Eastern Central Europe and do in general show heatwaves of lower duration between 6-9 days. The second lowest HWMId level (light grey color) with HWMId values larger than 3 and below 6 are mostly seen over Russia with short duration as well ranging from 3 to 9 days.

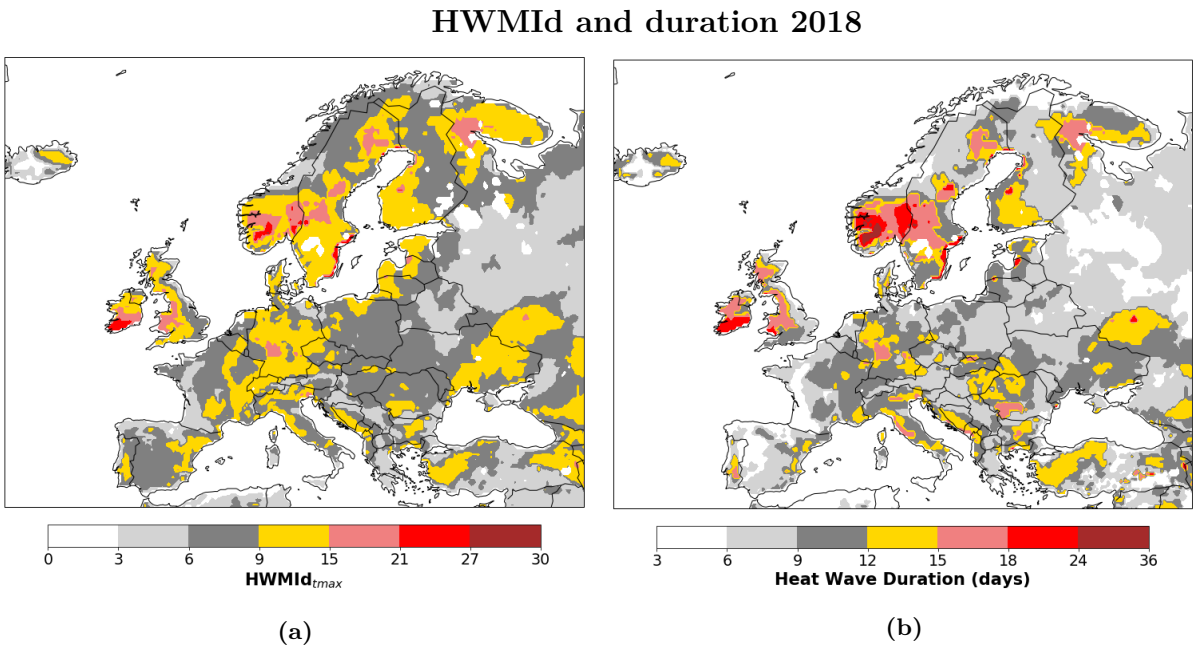

Figure 4.5: (a) Spatial distribution of the HWMId using daily Tmax. (b) Associated heat wave duration days

The starting months for the maximum heat waves in 2018 based on Tmax related to Figure 4.5 is displayed in Figure **??** below. The first maximum heat wave episode is present during April (pink) in Eastern, Southeastern and Southern Europe. In May, the maximum heatwave appear mainly in Southern Norway (except in the very south and Eastern part of Norway) and in some

parts of Southern Sweden (grey). Most of the British Isles experiencing the yearly strongest heat wave in June (green). The rest of Scandinavia and Finland, Spain and large parts of Central western Europe have the strongest heat waves in July blue). The strongest heat wave in Portugal are found in September (beige).

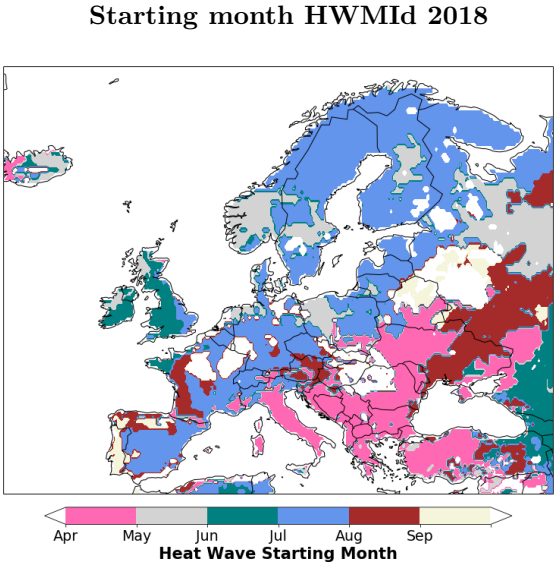

Figure 4.6: Starting month of strongest heat wave in 2018 from HWMId based on Tmax. White areas are starting months outside of the thesis scope

4.2.2 Daily minimum temperature (Tmin)

The map in Figure 4.7 shows the HWMId based on daily minimum temperature shows which places which has the highest night temperature which is mostly happen in July. The plot shows high night temperature in middle- and northern Norway, as well as the Stockholm region and the area around the Baltic Sea. Furthermore, it appears to be spots of high night temperature around highly density areas as e.g. Barcelona, Valencia, Palma de Majorca, Milan, Venice, Naples, Lyon, Montpellier, Prague, Vienna, Zurich, StraÃ§burg, Hamburg, Munich, Leipzig and Istanbul.

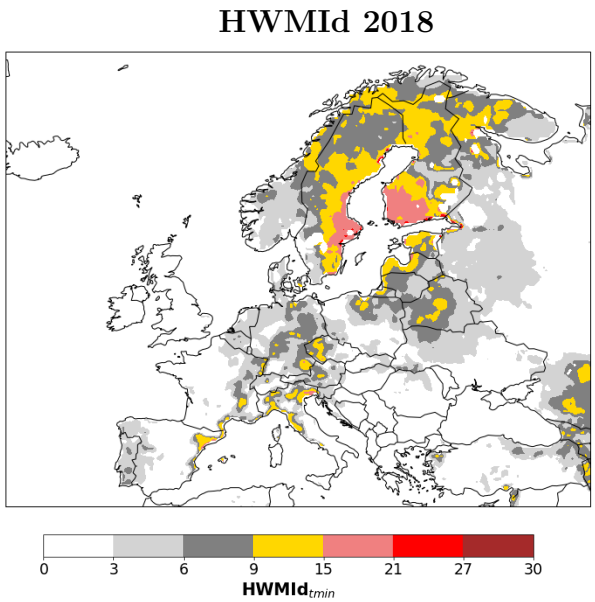

Figure 4.7: Spatial distribution of the HWMId using daily Tmin.

4.3 Monthly evolution in atmospheric blocking

The monthly evolution in the frequency of blocked days anomalies estimated from the AGP blocking index (see Section 3.4) and anomalies in the Z500 are visualized in Figure 4.8. Higher (positive) anomalies of approximately 4-6 days are shown over Greenland extending over Iceland and to the west coast of Norway in April (4.8 (a)). In May, a strong anomaly of approximately 14-16 days is centered over the Baltic Sea with corresponding high anomalies of around 175 in the Z500. Some weaker, but still high positive blocking anomalies are identified over the Southern part of Scandinavia in addition to Finland and north of the British Isles and further south in the Atlantic Ocean (35 ° to 45° N, 60 °W to 40°W) (4.8 (b)). Positive anomalies of approximately 7 days are seen west for the British Isles in June with Z500 anomalies of 75 m. Some positive blocking anomalies of nearly same magnitude are also seen south in the Atlantic Ocean west of the Iberian Peninsula (having weaker Z500 anomalies of 35 m) (4.8 (c)). High blocking activity with corresponding high anomalies in the Z500 (about 70 to 140 m) are located East for Scandinavia in July mostly fixed over Finland (4.8 (d)). The highest anomalies present there reaching as much as 24 more days of blocking compared to the climatology in which shows blocked days less than 5 days (Appendix 7.2 (d)). August bear little signs of abnormally blocking (4.8 (e)).An area of positive anomalies in blocking of approximately 6 to 10 days are located North West of Spain in September (4.8 (f)).

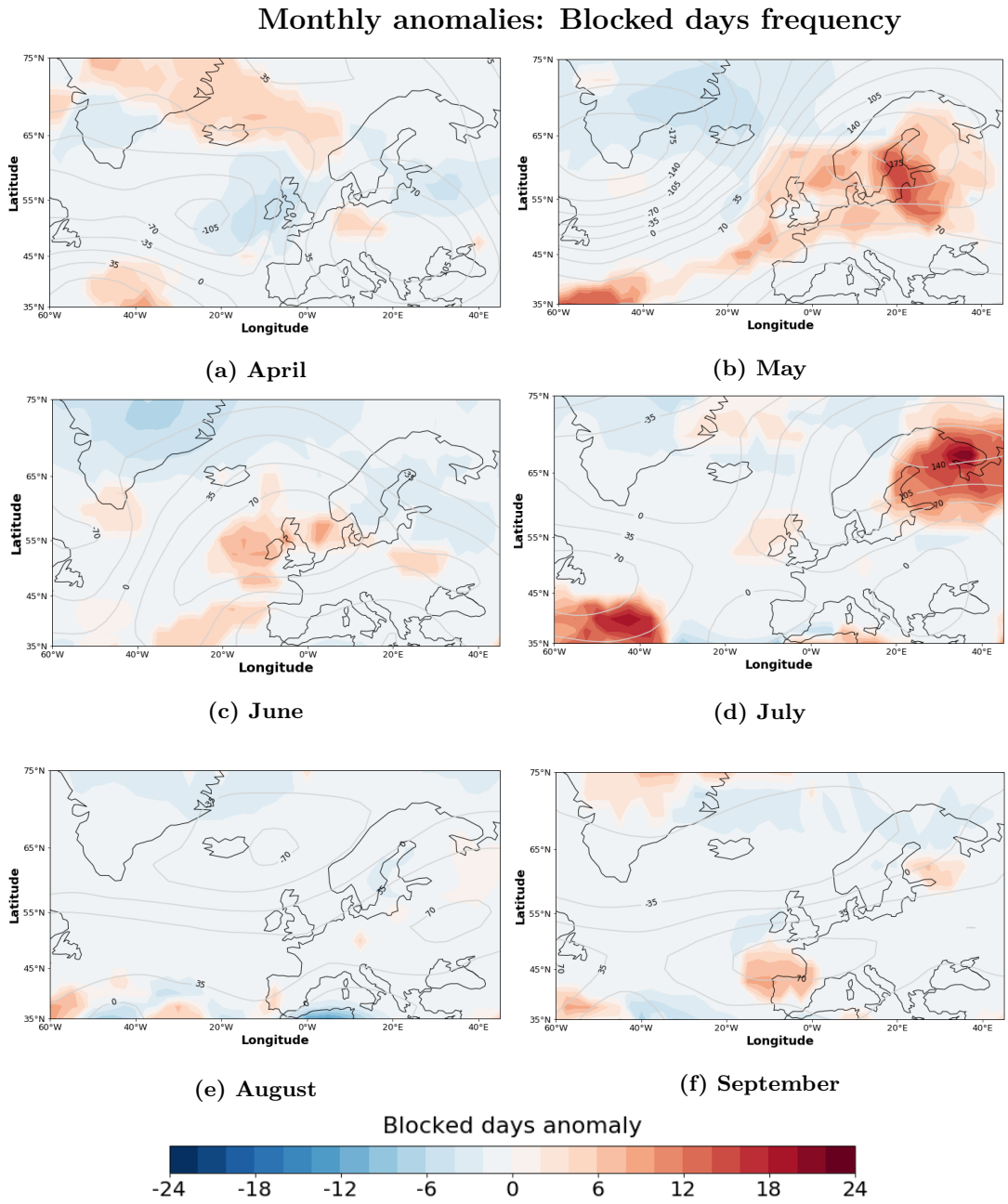

Figure 4.8: Two dimensional (2D) blocking index named "absolute geopotential height" (AGP) based on the study by Scherrer et al. (2006). Here we use geopotential height at 500 hPa data from the ERA5 reanalysis, interpolated into a 2.5 ° x 2.5 ° grid and display blocking days anomaly with respect to the climatology 1981-2010 over the European-Atlantic region: 60 °W - 45 °E, 30°N - 75 °N during April-September. The coloured shading shows the blocking days anomaly and the grey contours are the geopotential height anomaly at 500 hPa.

4.4 Soil moisture-temperature feedback

Monthly evolution of the correlation coefficient between soil moisture (SM) and latent heat flux (LHF) (terrestrial segment) is displayed in Figure 4.9. In April, SM shows a high negative correlation with LHF over mainly Central, Eastern and Southeastern Europe. Positive very high correlations can be observed for Eastern Spain and Turkey which is seen throughout all months (4.9 (a)). In May (4.9 (b)), high significant negative correlation is dominating in Northern Europe. Low to moderate positive correlations are observed over nearly the entire Sweden, Southern Finland and in the very Eastern part of Norway in June (4.9 (c)). In July, high positive correlations are confined to the southern part of Sweden and extending over a larger area in Eastern Norway including parts of Central Europe as well in (4.9 (d)). High positive correlation can be identified in the Eastern Europe in August, with moderate to high negative correlation and no correlation in Northern Europe (4.9 (e)). In September, very high negative correlation could be identified in Spain (4.9 (e)).

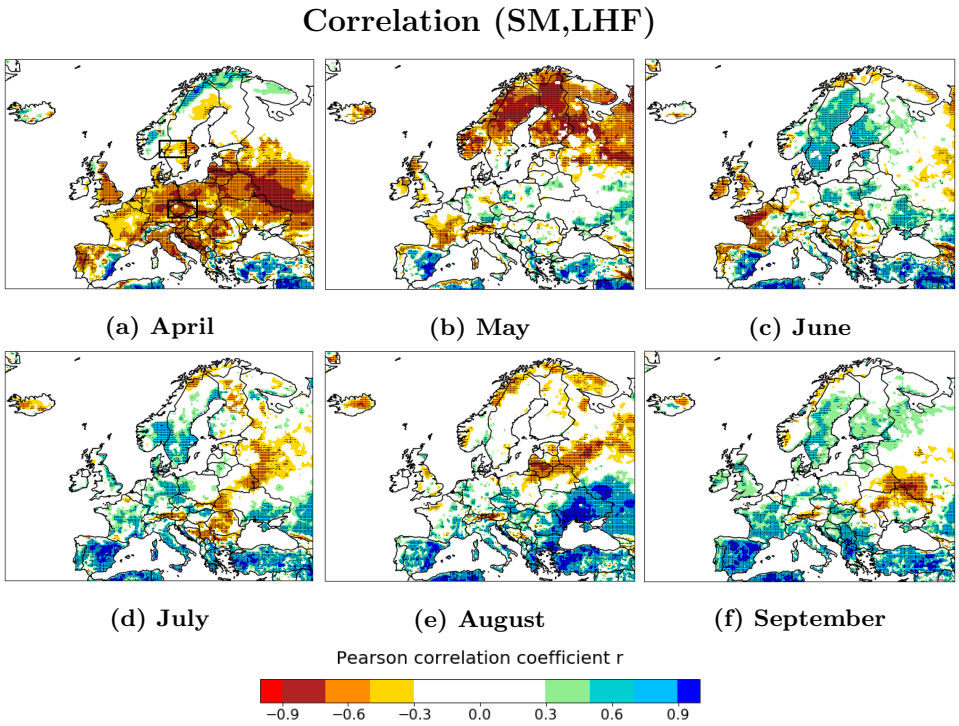

Figure 4.9: Pearson correlation coefficient between soil moisture (short: SM) and the latent heat flux (short: LHF) (terrestrial segment) for 2018 daily mean values from April to September. Blue colors indicate a linear positive association, whereas the red colors indicate a negative association. The black dots shows where the correlations are significant with $p < 0.1$. The two boxes plotted on top of (a) shows the two regions picked for regional analysis of energy budget in Subsection 4.4.1

Monthly evolution of the correlation coefficient between LHF and temperature at 2m (T2m) (atmospheric segment) is displayed in Figure 4.10. In April and May (4.10 (a) and (b)), positive significant correlations are mostly seen over Europe, except in April in Northern Europe where it shows either low negative or no correlation, except for Southwestern Europe (mainly Turkey) shows moderate negative correlation. Low to moderate positive correlations are observed over nearly the entire Southern Sweden, Southern Finland and in the very Eastern part of Norway in June (4.9 (c)). In July, moderate significant negative correlation can be seen in Southern Sweden, Eastern Norway and in the Czech republic and Eastern Europe is dominated by high positive correlation (4.9 (d)). August are mostly dominated by positive correlations, where high significant correlations are seen e.g. in the Eastern Europe (4.9 (e)). Positive correlations control much of the pattern in September as well, but some negative correlations can be recognized in for instance Southern Finland and different locations in Spain (4.10 (f)).

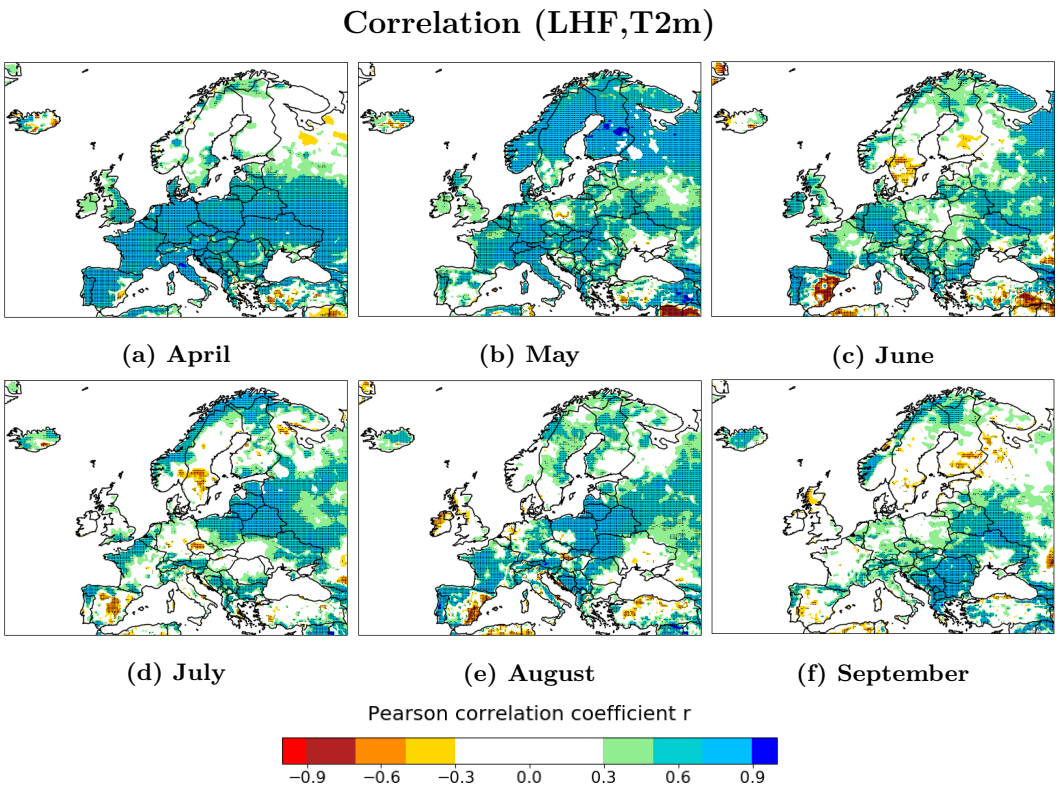

Figure 4.10: Monthly spatial distribution of the Pearson correlation coefficient r between latent heat flux (short: LHF) and the 2m air temperature (short: T2m) (atmospheric segment) for 2018 daily mean values. Blue colors indicate a linear positive association, whereas the red colors indicate a negative association between LHF and T2m, in which the exact correlation levels are defined in Section 3.5. The black dots shows where the correlations are significant with $p < 0.1$.

Monthly evolution of the correlation coefficient between SM and T2m is displayed in Figure 4.11. Negative correlations are mostly seen for all successive months, except from April in which positive correlations are found in the Northern countries (mostly high correlations) (4.11 (a)). In May, high to very high negative correlations are centered around Northern Europe and Central Europe (4.11 (b)). Very high negative correlation is observed over Spain in June, and high positive correlations are seen in many other places like e.g Southern Norway and Sweden Europe (4.11 (c)). No correlation/negligible correlation are seen in most parts of e.g. Southern Sweden and Norway in July (4.11 (d)). A high positive correlation are in August mostly seen in large parts of Central Europe, North West Russia and East coast of Spain (4.11 (e)). Very high correlations are seen over Russia in September and high correlations are extending over the Central Europe. Moderate correlations can be detected e.g. in Finland. (4.11 (f))

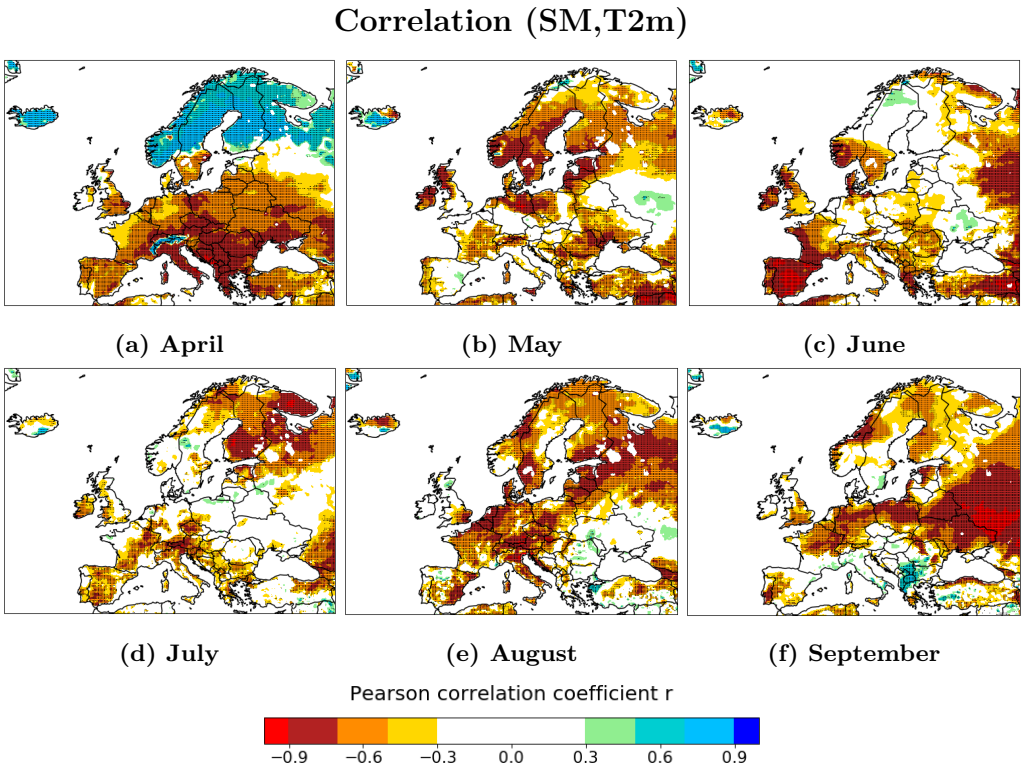

Figure 4.11: Pearson correlation coefficient between soil moisture (short: SM) and the 2m air temperature (short: T2m) for 2018 daily mean values from April to September. Blue colors indicate a linear positive association, whereas the red colors indicate a negative association between SM and LH, in which the exact correlation levels are defined in Section 3.5. The black dots shows where the correlations are significant with $p < 0.1$.

4.4.1 Regional heat budgets

Figure 4.12 below shows monthly anomalies for 2018 of energy fluxes including the 2m temperature (heat budget). The anomalies are averaged over two European land areas referred to as: "South-Norway-Sweden" and "Czech Republic". The black boxes in Figure 4.9 (a) displays the respective areas.

Figure 4.12 (a) shows the energy budget for "South-Norway-Sweden". The anomalies in the turbulent fluxes (blue) and the respective components of sensible (orange edge) and latent heat flux (blue edge) are initially negative and small anomalies in the net top of the atmosphere (TOA) (red), net surface radiation (purple) and temperature near surface (black and white hatched) are seen in April. The largest temperature anomaly is seen in May with a temperature anomaly of approximately $+5\ ^{\circ}C$. A small positive anomaly of approximately $+4\ \frac{W}{m^2}$ in the latent heat flux and approximately $+8\ \frac{W}{m^2}$ for the sensible heat are seen in May with large anomalies in the net TOA and net surface radiation as well. In June, the latent heat flux anomaly is slightly negative and the sensible heat flux has increased to approximately $25\ \frac{W}{m^2}$ accompanied by lower temperature (approximately $+2\ ^{\circ}C$). In July, the anomalies in the radiative fluxes have increased, and a large negative anomaly of approximately -20 $\frac{W}{m^2}$ in the latent heat flux and approximately $+40\ \frac{W}{m^2}$ in the sensible heat flux are identified. The temperature peak is slightly less than for May (approximately $+4.5\ ^{\circ}C$). All fluxes close to climatology in August and September (see Appendix 7.6).

Figure 4.12 (b) displays the energy budget for "Czech Republic". In April, the anomalies in the turbulent fluxes (blue) and the respective component of sensible heat flux (orange edge) is initially slightly negative and the second component of latent heat flux (blue edge) is initially quite large (approximately $+15\ \frac{W}{m^2}$. A large temperature anomaly of approximately $5\ ^{\circ}C$ is seen as well. Anomalies in net radiation at TOA and at surface are approximately +15 and $+20\ \frac{W}{m^2}$ both in April and May. In the evolution over the months one can observe a gradually decrease in latent heat flux anomalies and peaks at approximately -18 $\frac{W}{m^2}$ in August. The opposite is seen for the sensible heat flux, where this flux gradually increases in magnitude and peaks at approximately $+25\ \frac{W}{m^2}$ in both July and August. In September, all anomalies in fluxes including temperature are much lower.

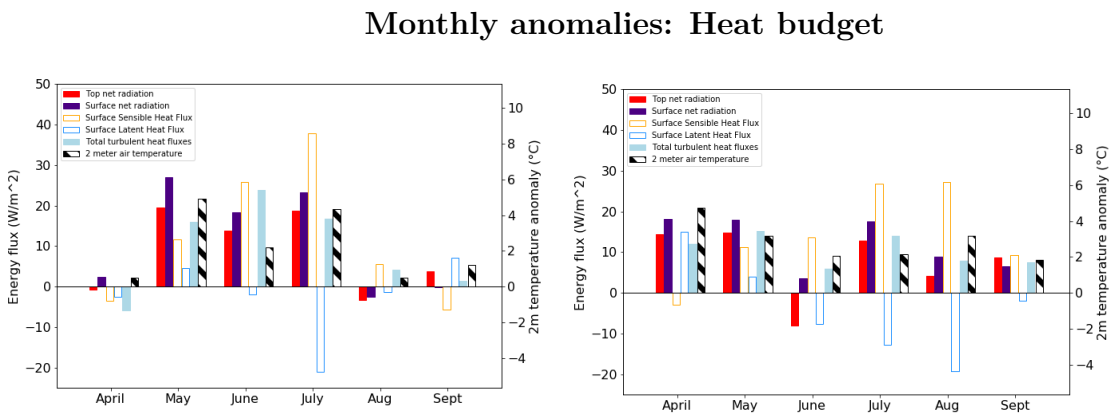

(a) South-Norway-Sweden **(b)** Czech Republic

Figure 4.12: Anomalies with respect to the climatology 1981-2010 from April-September 2018 in: TOA net radiative flux (red), surface net radiative flux (purple), surface sensible heat flux (orange edge), surface latent heat flux (blue edge) and surface turbulent flux (sensible + latent heat flux) (blue) and temperature at 2m height (black and white hatched). The anomalies are averaged over the regions: (a) 10-16 °E, 58.5-61 °N (b) 10.5-17 °E , 49-52 °N. The boxes showing the areas are plotted on top of Figure 4.9 (a). The radiative fluxes are defined positive downwards, whereas the turbulent fluxes are defined positive upwards. The Figure idea is inspired by the study of the 2003 European heatwave by Black et al. (2004).

5 | Discussion

5.1 Monthly evolution of the 2018 European heat wave

5.1.1 April

Eastern, Southeastern and Southern Europe experienced the strongest heat wave in 2018 in April according to HWMId (Tmax). HWMId (Tmax) showed maximum values between 9 to 15 (mostly in the Southern Europe) with a duration of about 2 weeks (Figure 4.5). Compared to the HWMId (Tmax) from the 2003 European heat wave (see Theory Section Figure 2.1 (a)) the HWMId of 9 to 15 could be seen in parts of Spain and surrounded also a much stronger area in France where the maximum peak reached 48. Thus, the 2018 European heat wave in April can be comparable with the 2003 European heat wave to some extent. Not as strong as the most affected areas in 2003, but the two events were approximately having same duration (Figure 2.1 (b)).

The main driving mechanism that triggered this heat wave can be connected to the anomalously anticyclonic circulation in the Z500 field in which yielded fair weather conditions at surface with less precipitation and soil moisture than usual. The question is whether soil moisture interactions with the atmosphere was present or not in contributing to the high temperatures. Based on currently knowledge about this mechanism (see Theory Section 2.3.3), a strong positive terrestrial feedback could essentially be expected to see in the Southern Europe. Since the correlation between soil moisture and latent heat flux (the terrestrial segment) showcased significant positive values (very high especially in Turkey) (Figure 4.9 (a)), this might implies that the soil moisture controlled the latent heat flux in the Southern European region (a state of soil moisture limited regime) in which is a necessary condition in the further investigation of an eventually strong positive land-atmosphere coupling. A moderate significant negative correlation between the latent heat flux and the temperature (the atmospheric segment) could be seen in some areas in the Southern Europe (mostly in Turkey) (Figure 4.10 (a)), suggesting that the temperatures are not damped by any further increase in latent heat flux and more energy is

available for sensible heat which amplifies the temperatures. The atmospheric segment for rest of South Eastern and Eastern Europe was dominated by high positive correlations which might implies that the higher temperatures resulting from the increased radiation increased the latent heat flux (a cooling effect) due to higher vapour pressure. This effect combined with moderate to high negative correlations of the terrestrial segment led to a further decrease in the soil moisture. Therefore, despite the whole area of the strongest heat waves showed significant negative correlation between the soil moisture and temperature (Figure 4.11 (a)), the physical mechanisms behind were different.

From the monthly mean temperature anomalies, one could also recognize that Central Europe was exceptional warm in April. This was evident from the regional heat budget averaged over the Czech republic (4.12) where this area gained high positive anomalies in the net radiation at TOA and surface that supplied a lot of energy heating the atmosphere near surface and increased the latent heat flux, but sensible heat flux was negative most likely due to the fact of a state of energy limited evaporative regime as the case for Eastern and Southeastern Europe discussed above.

5.1.2 May

The HWMId (Tmax) captured the strongest heat waves mainly over the Southern Norway and parts of Southern Sweden which we have seen had exceptional high daily mean temperature anomalies. The HWMId (Tmax) showed values from about 18 to 27 in Southern Norway (a very small peak of 27 to 30 could also be seen), but only 9 to 15 in Sweden. Compared to the HWMId from the 2003 European heat wave (Figure 2.1 (a)), the HWMId of 18 to 27 in Norway can be treated quite extreme, but the very small spot of 27 to 30 is not as strong as the strongest peak in 2003 which was 48. However, the heat wave in May was exceptional in duration, where the heat wave in Southern Norway reached almost 36 days in which compared to Western Europe in 2003 had a maximum duration of 18 days (Figure 2.1 (b)) which is more similar with the heat wave in Sweden this month.

Anomalously anticyclonic circulation in the Z500 field was dominating these areas with persisting atmospheric blocking frequency might associated with a Scandinavian blocking regime with lower pressure to the south. When such long persistent blocking highs are placed over the same area for such a long time, the usual low pressure systems coming from west were blocked over a long period of time which most likely brought some positive anomalies in precipitation seen further north in Norway. Despite the high negative correlation between soil moisture and temperature seen in Northern Europe, the terrestrial correlation segment was moderate to

high significant negative in Southern Norway which might suggesting that the high frequency of blocked days associated with anomalously positive radiation were the driver for the extreme temperatures contributing to an eventually increase in the latent heat flux that decreased the soil moisture content (a state of soil moisture energy limited regime) since the increase of air temperature increases the vapour pressure which might have increased the latent heat flux even more and further contributed to gradually drying the soil. Surprisingly, this was not the case for Southern Sweden in which showed no linear relationships of the terrestrial segment.

The same findings from the correlations of the two segments of the soil moisture-temperature feedback discussed above could also be reflected in the regional heat budget averaged over Eastern Norway and Southern Sweden. The exceptional high anomalies in the net radiative fluxes on TOA of approximately + 20 $\frac{W}{m^2}$ and surface of approximately near 30 $\frac{W}{m^2}$ can be connected to the persistent Scandinavian blocking with clear skies in which heated the atmosphere over a long period of time and since higher temperatures increases the evaporating demand this resulted in an increase in latent heat flux in which further decreased the soil moisture, but this latent heat flux anomaly was rather small (approximately +4 $\frac{W}{m^2}$) which might can indicate that soil moisture is not far from a state of a transitional soil moisture regime where it can start controlling the latent heat flux.

5.1.3 June

An overall clearly weakening in the temperature anomalies were seen and the Scandinavian blocking had dissipated where a shift in the upper air flow was evident. According to the HWMId (Tmax), the strongest heat wave over the British Isles started this month. The HWMId over the British Isles showed nearly similar values compared to Southern Norway in May, where the highest values of 21 to 27 could be identified in Southern Ireland and 9 to 21 along the western part of Britain. Even though lower daily mean temperatures were present over this area in June , the HWMId shows high values like the case for Southern Norway, but the long duration of approximately 15 to 24 might partly explain the high HWMId values.

Over this region, positive atmospheric blocking anomalies were identified, but fewer days of blocking were present compared to the very persistent Scandinavian blocking seen from May combined with much lower Z500 anomalies as well. Consequently, the temperature anomalies were not exceptional here, but slightly less precipitation than usual and an approximately 5 % negative anomaly in the soil moisture could be seen over Britain and a general decrease in soil moisture over Northern Europe as well. The same arguments of the soil moisture-temperature feedback drawn from Southern Norway can be transferred to the British Isles where meteoro-

logical features most likely contributed to control the latent heat flux where the soil moisture were confined to a energy limited regime in which the blocking and soil moisture drying were not co-interacting to enhance temperatures. Another important incident worth mention, is a change observed for the regimes of soil moisture controlling of latent heat flux in Scandinavia. The terrestrial segment of the soil moisture-temperature feedback over Sweden including southern Finland and a small part of Eastern Norway as well have changed to positive correlation which might indicate that soil moisture has got dry enough to starting limiting the latent heat flux (within the transitional zone). For the atmospheric segment, the negative correlations are most pronounced for Southern Sweden, but includes a small part of Eastern Norway and Southern Finland as well This may indicate a presence of increased sensible heat flux with a decreasing of the latent heat flux. However, due to the weak pressure anomalies the co-interaction was likely small in the presence of higher temperatures.

Again, pointing to the regional heat budget over Southern Sweden and Eastern Norway, the indication that soil moisture entered the latent heat flux soil moisture limited regime and more energy available for sensible heating can be identified from the shift from the positive latent heat flux anomaly from May to a slightly negative anomaly in June (approximately $-2\frac{W}{m^2}$ in June), and the increase in the sensible heat flux anomaly from May to June approximately ($+20\frac{W}{m^2}$ in June). The small anomaly in latent heat flux might indicate that the land-atmosphere coupling is quite weak as for now and in combination with the smaller anomalies in the radiative fluxes which is most likely due to the smaller pressure anomalies, a weak positive peak in the temperature is seen.

5.1.4 July

From the HWMId (Tmax) values, the strongest heat waves in July seem to be starting in Northern Europe, Western Europe, Central Europe including Spain as well. However, with respect to duration the most prolonged heat waves from this month were restricted to the Southern parts of Norway and Sweden.

Long lasting Scandinavian blocking were again identified, but this time even higher anomalies of blocked days were detected and was centered mainly over Finland, but slightly lower anomalies in the Z500 compared to May were seen, but covering a larger area over Northern and Central Europe. Due to the presence of anomalously high blocking and large areas of high positive anticyclonic anomalies, it is thus interesting to investigate whether co-interaction with land-atmosphere couplings were present to explain the exceptional heat waves. Despite the presence of large areas of positive terrestrial correlations, low to high negative correlations were only

seen in some few areas mainly in Southern Sweden, Eastern Norway, the Czech Republic and Spain. The reason for a non existing linear relationships between soil moisture and temperature in the Southern parts of Sweden and Eastern Norway could might be due to the fact that soil moisture was approximately dried out at some point or which was also evident from the very large anomalies or that the temperature stabilized at its high values.

According to the heat budget averaged over Southern Sweden and Eastern Norway, the strong land-atmosphere coupling from the discussion above between soil moisture and temperature could be clearly identified with exceptional peaks in the turbulent fluxes in which the latent heat flux anomaly reached as small as approximately $-20\frac{W}{m^2}$ and sensible heat flux approximately almost 40 $\frac{W}{m^2}$. This further showcase that there might was a strong interlinkage between anomalously radiative fluxes due to the Scandinavian blocking regime and the effect from the soil moisture drying which was transferred mostly as sensible heat flux from the surface into the atmosphere contributing to raise the temperatures near surface. The decrease in latent heat flux was also recognized in the heat budget averaged over the Czech Republic, but not as large anomaly (approximately 12 $\frac{W}{m^2}$ as seen in Northern Europe which might indicate a stronger soil moisture-temperature feedback in Northern Norway.

Figure 4.7 in the results shows where the night temperature was highest during the heat wave in July. The map indicates a correlation between high nighttime temperatures and densely populated places. It looks for example like Barcelona, Hamburg, the Stockholm region, Prague and Munich are hit by extra high night temperatures. This corresponds well with the Urban Heat Island phenomenon, which indicates that the night temperature in densely populated urban areas is higher than the average temperature otherwise. Although the correlation is not perfect and there are obviously other phenomena that are more important in a heat wave, it is a causation of warning. The negative effects of hot temperature are exponential (e.g. a 5 degree increase from 35 to 40 degrees is much worse than a 5 degree increase from 20 to 25 degrees). When more people immigrates to big cities at the same time the results may indicate that densely populated areas are hit hardest by a heat wave, this is something that should be closely monitored for future adaptions.

5.1.5 August and September

In August, the disruption of the westerlies that caused the long persistent atmospheric blocking regime over Scandinavia seen in July became more zonal again and low pressure systems coming from from west brought precipitation which supplied the exceptional dry soil from July with moisture. Simultaneously, positive anomalies in the Z500 were still found over Central Europe

which maintained the negative anomalies in the soil moisture over these areas. This was evident from the regional analysis in the Czech Republic in which the latent heat flux reached the maximum negative peak of approximately the same value as for Southern Sweden and Norway in July (see previous discussion on July).

According to the HWMId (Tmax), there was no particularly strong heat wave which started this month, but In September Portugal experienced its strongest heat wave with HWMId values of 6 to 15 with a duration of about to weeks. A weak blocking could be identified over Southwestern Europe. From the correlation analysis related to the soil moisture- temperature feedback, the correlation between soil moisture and temperature over Portugal was negative in the Southern part in September. Even though the terrestrial segment showed positive correlations, the atmospheric segment was positive indeed which might imply that due to the anomalously blocking might increased the latent heat flux which reduced the soil moisture anomalies.

6 | Summary and conclusions

In this section, the most central findings from the results are presented and some practical implications of heat waves are given. The latter also includes a brief discussion of what effects e.g. climate change and new settlement patterns will have for the future.

6.1 The 2018 European heat wave

The 2018 European heat wave was not a single phenomenon which was constant throughout Europe. Rather, this thesis has shown the evolution of heat waves and drought in different places at varying magnitudes from April to September. Several factors were important, and both large-scale patterns of blocking highs and soil moisture-temperature feedback the anomalously high temperatures were mainly caused by the evolution of anomalously positive pressure conditions helped explain the anomalously high temperatures and duration. Nevertheless, this thesis indicates that the anomalously high temperatures were mainly caused by the evolution of anomalously positive pressure conditions. The reanalysis data from ERA5 presented indicates that the strongest and most persistent heat waves were mainly identified in Northern Europe. In Scandinavia, the data presented indicates that there were two main peaks of the heat wave, one in May, and one in July.

As a result of anomalously positive anticyclonic pressure patterns, a strong heat wave appeared over Central, Eastern, Southeastern and Southern Europe in April. The anomalously high temperatures in Southern Europe were found to be an interlink between higher pressure conditions and soil moisture drying enhancing temperatures, whereas the remaining places could mainly be explained from higher pressure anomalies. The heat wave developed further towards Northern Europe in May, particularly to Southern Norway and Sweden, as we got the first peak in temperature in May. Here, the monthly mean temperature peak was approximately 6 $^{\circ}C$ above the climatology, and exceptionally high anomalies in net radiation that heated the surface and increased the latent heat flux contributed to soil drying. These factors in May indicate that

the Scandinavian blocking was an important driver for the first heat wave peak we found in May. The main difference between the first heat wave in April and the second heat wave over Scandinavia was that the first was associated with high anomalies in pressure field rather than atmospheric blocking, which was present over Scandinavia in May. The main implications of the latter is that when a high pressure system is situated over the same area for a long time it can steer the usual west to east cyclones in combination with continuously sinking of air masses which produce stable fair weather for prolonged periods of time. This shows that there are various factors that provoke a heat wave, but also that soil moisture drying can enhance the effect as seen in Southern Europe. In June, the blocking from May was absent over Scandinavia, but a strong heat wave lasting for 9 to 24 days over the British Isles was placed below an atmospheric blocking regime which could partly explain the prolonged heat wave. However, the soil moisture continued to decrease in the Northern Europe and started to limit the latent heat flux. Further, only in particularly Southern Sweden and a small part of Eastern Norway an atmospheric response in temperature from soil drying was observed where the latent heat flux anomalies turned slightly negative and sensible heat flux increased. However, due to the absent of high pressure anomalies, the second peak was seen in July where a high frequency of anomalously Scandinavian blocking regime was again appearing and could be seen in light of an interlinkage with the negative soil moisture anomalies. From the regional heat budget over Southern Sweden and Norway, exceptional negative anomalies in latent heat flux of approximately -20 $\frac{W}{m^2}$ and sensible heat flux of +40 $\frac{W}{m^2}$ could be detected. The monthly mean average temperature was approximately 5 $°C$ above the climatology. Although June was somewhat milder than the two summits discussed earlier, it is important to note that it was still very hot in most parts of Europe. Although, in meteorology, specific terminologies are used to define heat waves and their peaks, it is important to mention that the perceived feeling by many was a constant high temperature where the desiccation caused ever-worse crops and other negative consequences. The conditions for many people were therefore significantly less desirable than if they were only to be seen as two separate events.

Due to a shift in the upper level flow, where the westerlies approached more zonal (connected to the Rossby waves), the Scandinavian blocking regime dissipated and the west to east cyclones which brought precipitation to Northern Europe and soil moisture returned to approximately normal conditions. Therefore, in the vast majority of Europe there was decreasing heat in August and September. The outlet was Central Europe, where positive anomalies were still present due to higher pressure conditions and Portugal, which in September experienced a heat wave as a result of anomalous pressure in combination of blocking which could be identified in the Atlantic Ocean outside of the Iberian Peninsula. In other words, there was not a real heat wave in most

parts of Europe during those months, although it may have been experienced this way for many. However, for the reasons discussed in the section above, it may be worth noting that the weather may have felt worse for many than if there were such temperatures in August and September for another year without the previous / underlying heat wave. And even in August and September, temperatures in Europe far exceeded an average year.

When we look at the interlinkages between the mid-troposphere circulation and the soil moisture-temperature feedbacks, the main findings are that they are able to greatly influence each other. One of the reasons why the heat wave in July was stronger in Eastern Norway and Southern Sweden compared to May could be explained by the gradual soil drying that reached a state of soil moisture limited regime and was able to control the latent heat flux and thereby contributing to a strong land-atmospheric interaction influencing the temperature. The implications of one peak being able to launch and reinforce new peaks have major implications, as society is much better equipped to deal with short-term extremes, than long-term weather abnormalities.

6.2 The bigger picture

We have seen that the heat wave in 2018 bears similarities to previous heat waves. The 2018 European heat wave in April can be compared to the 2003 European heat wave to some extent, and the two events had approximately same duration. The strongest peak in the HWMId from 2003 was between 36 and 48, and the HWMId peak from the 2018 computed from this thesis was between 27 and 30he 2018. However, the 2018 European heat wave was exceptional in the sense of its long duration, prolonged drought and prevalence. Similarities of characteristics with the 2003 heat wave could also be drawn from the regional heat budgets conducted for the heat wave in 2018. The main similarity which could be seen was that the negative soil moisture anomalies induced negative latent heat flux anomalies for all three heat waves where more energy was available for sensible heating, but 2018 in "Southern-Norway-Sweden" and "Czech Republic" were characterized by higher magnitudes in latent heat flux compared to 2003 of a maximum negative anomaly of approximately -8$\frac{W}{m^2}$ compared to 2018 of approximately -20$\frac{W}{m^2}$ (bear in mind that different datasets and climatology are used).

The results showed a correlation between population density and high night time temperatures, e.g. in Barcelona and Hamburg. Due to the fact that heat absorbed during the daytime is released as long wave radiation in the evening and during night time, heat waves can cause serious problems especially in highly populated areas due to many complex and combined factors.

At its warmest, during the heat wave in 2018, it was 7 degrees warmer on a monthly average than normal, which has major complications in urban areas where it is already warmer than average. More than half of the world's population lives in urban areas, in excess of 4 billion people, and this continues to increase. A UN report estimates that by the year 2050, 68 percent of the world's population will live in urban areas (Nations, 2018). Although this thesis has addressed the European heat wave in 2018, heat waves are a global phenomenon and just under 1-in-3 people in urban areas globally live in a slum household (Ritchie and Roser, 2018). This is an extra caution of warning.

The fact that more and more people are experiencing warmer temperatures, combined with a general growth in prosperity in the world, can further lead to more warming e.g. due to the purchases of air-conditioning appliances, which in turn emit harmful greenhouse gas emissions and amplify the aforementioned effects. There have been several heat waves in recent years, and nothing indicates that there will be fewer in the coming years. Global warming is causing the events described in this thesis to happen more frequently, and the consequences have been catastrophic at times. Far above 100,000 people have died of heat waves since the start of this millennium alone. Furthermore, heat waves lead to crop failure, wildfires and other damage to people and nature, and the topic is therefore very important to research, discuss and understand thoroughly. Understanding heat waves, and their associated effects, is therefore something that is not just important in meteorology, but the research influences will have impacts on fields such as immigration, climate research, economics, medicine, social anthropology and biology.

7 | Limitations and future work

7.1 Limitations

It should be mentioned that this study is not without limitations. As mentioned in the method chapter, reanalysis data based on modeling is used, not actual observations. Observations have their own limitations (for example, they may be deficient), but ideally both should be looked at in combination to get the most accurate picture of the European heat wave in 2018. The thesis also did not include other factors such as SST and altitude profiles of the atmosphere. Furthermore, even though the quality of soil moisture data has steadily increased, it still has uncertainties especially related to surface conditions (e.g. dense vegetation, organic soils), which can increase the uncertainty of the accuracy of the data (Dorigo et al., 2017). In addition, related to the correlation analysis conducted for the soil moisture-temperature feedback in this thesis one assumed the data was approximately normal distributed which might not be the case. Consequently, the two limits motioned might have affected the results. Due to resource constraints, the thesis has only looked at the soil moisture from the model top layer (0-7 cm), although there are also 3 other layers in the reanalysis data. The choice was based on the fact that the interactions are closest to the surface (Gao et al., 2019). When it comes to atmospheric blocking it has been interpolated from the original grid which is a fine grid (0.25° x 0.25°) to a coarser 2.5° x 2.5° which has a lower resolution. As mentioned in the theory subsection about blocking indices (2.2.4), one weakness with AGP is that stable semi-permanent anticyclones might be treated as blocked, although in reality these are not associated with a blocking phenomenon. This may have affected the result. Finally, it is worth mentioning that the task has only looked at monthly averages. Therefore, there is a possibility that one has missed effects or trends that have taken place between months, or only occurred for so few days that it does not appears significantly on the monthly average. It can also have the opposite effect, that strong effects that only apply for a shorter period leave behind the impression of applying for a full month.

7.2 Future work

Further research should address several of the aspects that this theisis, due to resource constraints, has not considered. Research should be done with observational data that will provide a supplementary picture of the European heat wave in 2018. Furthermore, the impact of other factors such as SST and altitude profiles should be researched. Other blocking indices, and other soil moisture layers, are factors that this task has not addressed, but which it would be interesting to research further. Finally, in the thesis I briefly touched into the fact that it may appear that there is higher night temperature in areas with high population density. This can probably be linked to a phenomenon called Urban Heat Island (UHI), which says it is significantly warmer in urban places than its surrounding rural areas due to human activities. UHI is a complex phenomenon and many factors come into play. But because of the important implications (the damage of heat is exponential with high temperatures, more and more people are moving into big cities, etc.), this is an area that would have been very interesting with more research related to the 2018 heatwave.

A | Monthly climatology

7.1 Monthly evolution

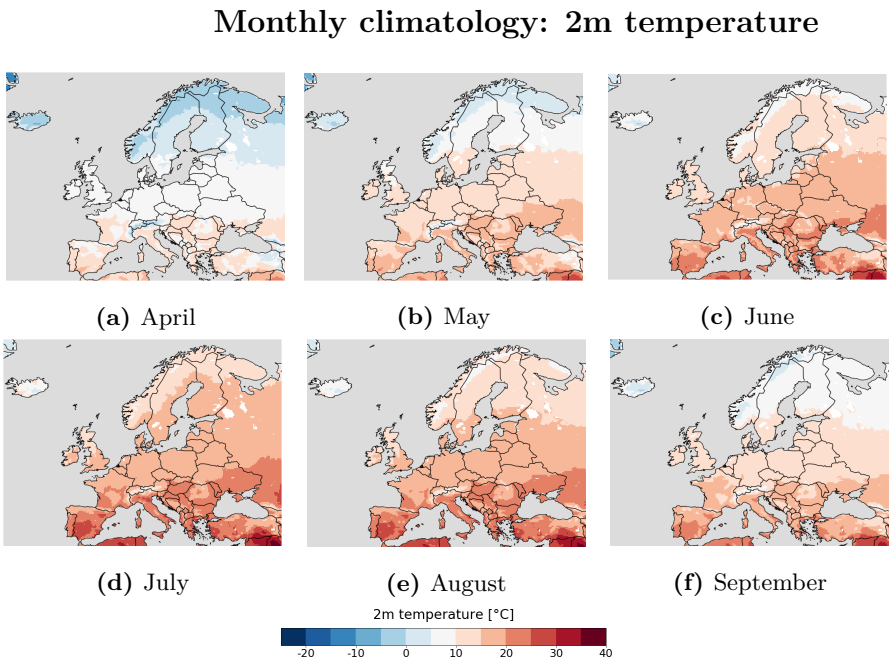

(a) April **(b)** May **(c)** June

(d) July **(e)** August **(f)** September

Figure 7.1: Climatology in continental air temperature 2 metre above the surface the months April to September 2018 (unit: °C).

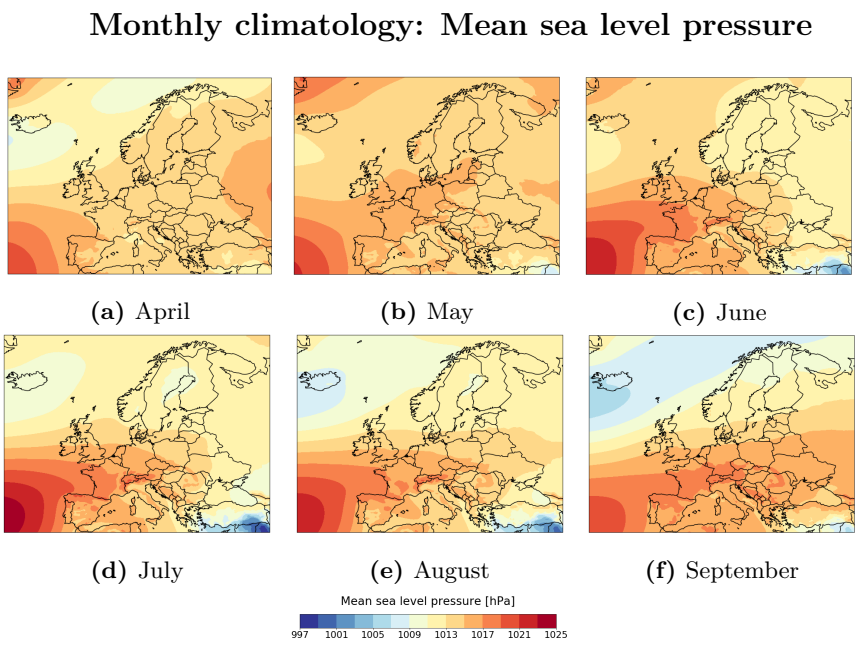

Figure 7.2: Climatology in the mean sea level pressurefor the months April to September 2018 (unit: hPa).

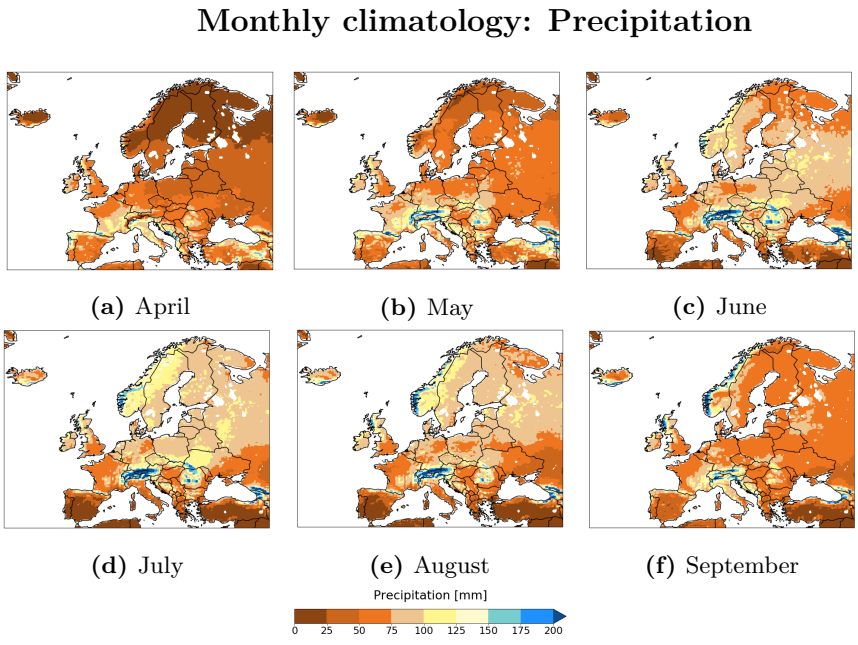

Figure 7.3: Climatology in the precipitation for the months April to September 2018. Total precipitation is composed of a sum of convective and large scale precipitation (unit: mm).

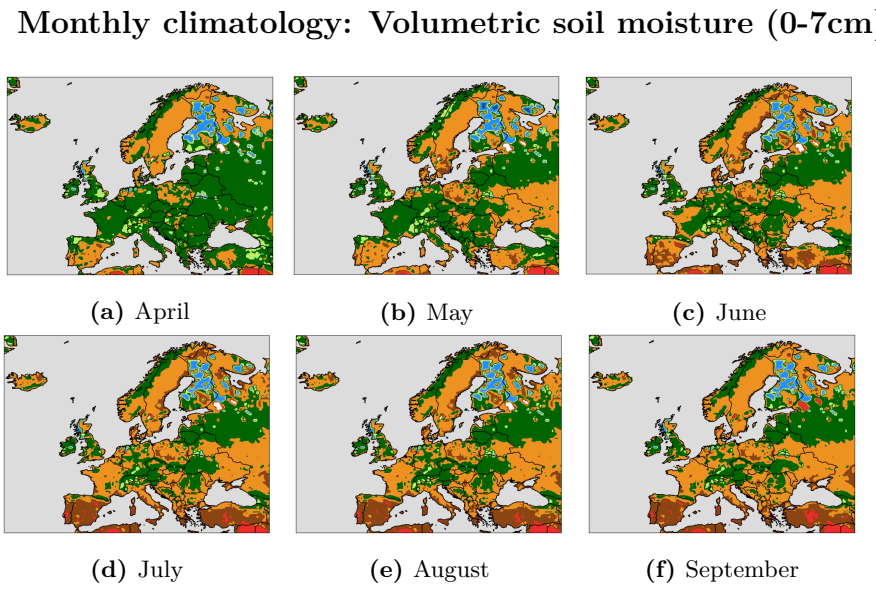

Figure 7.4: Climatology in the volumetric soil moisture content at surface (0-7 cm) for the months April-September 2018 (unit: %).

7.2 Atmospheric blocking index

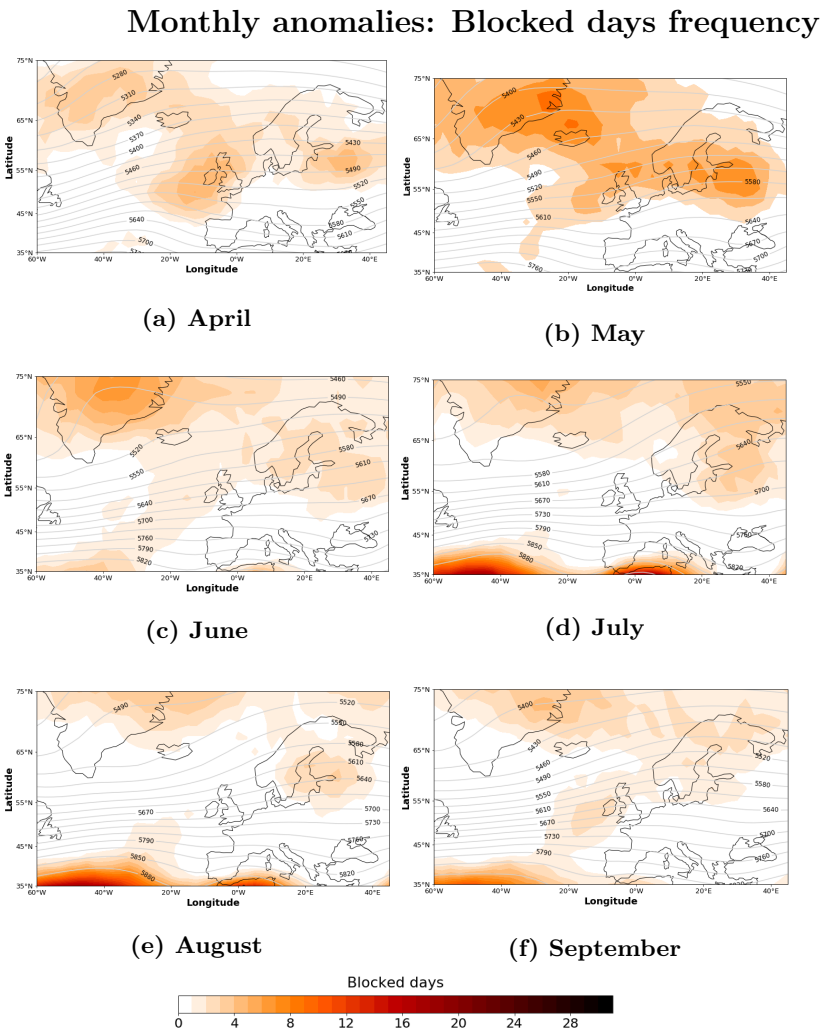

Figure 7.5: Climatology from AGP blocking index, based on the study by Scherrer et al. (2006) which display averaged blocked days anomaly with respect to the climatology 1981-2010 over the European-Atlantic region: 60 °W - 45 °E, 30°N - 75 °N during April-September

7.3 Regional energy budget

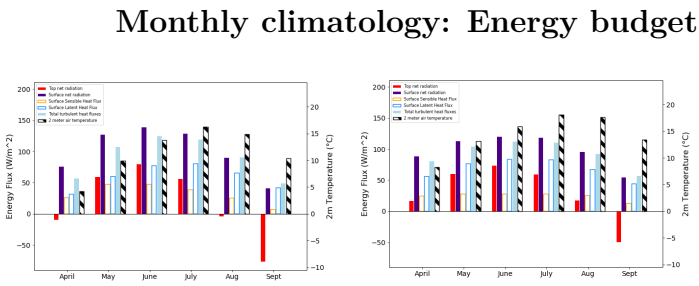

(a) South-Norway-Sweden **(b)** czech republic

Figure 7.6: climatology (1981-2010) from April-September in: TOA net radiative flux (red), surface net radiative flux (purple), surface sensible heat flux (orange edge), surface latent heat flux (blue edge) and surface turbulent flux (sensible + latent heat flux, lightblue) and temperature at 2m height (black and white hatched). The anomalies are averaged over the regions: (a) 10-16 °E, 58.5-61 °N (b) 10.5-17 °E , 49-52 °N. The boxes showing the areas are plotted on top of Figure ?? (a). The radiative fluxes are defined positive downwards, whereas the turbulent fluxes are defined positive upwards.

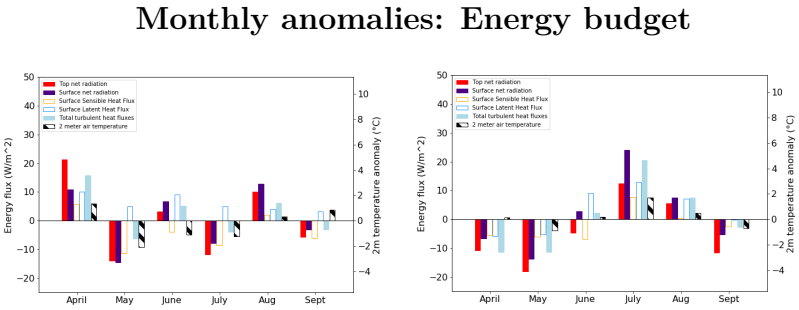

(a) South-Norway-Sweden **(b)** Czech Republic

Figure 7.7: Anomalies with respect to the climatology 1981-2010 from April-September 2013 in: TOA net radiative flux (red), surface net radiative flux (purple), surface sensible heat flux (orange edge), surface latent heat flux (blue edge) and surface turbulent flux (sensible + latent heat flux) (blue) and temperature at 2m height (black and white hatched). The anomalies are averaged over the regions: (a) 10-16 °E, 58.5-61 °N (b) 10.5-17 °E , 49-52 °N. The boxes showing the areas are plotted on top of Figure ?? (a). The radiative fluxes are defined positive downwards, whereas the turbulent fluxes are defined positive upwards. These showcase characteristics of a heat budget under non heat waves.

Bibliography

M. Allaby. Azores high, 2020a. URL https://www.encyclopedia.com/earth-and-environment/ecology-and-environmentalism/environmental-studies/azores-high. Last accessed June 08, 2020.

M. Allaby. anticyclone, 2020b. URL Encyclopedia.com:https://www.encyclopedia.com/science/dictionaries-thesauruses-pictures-and-press-releases/anticyclone-0. Last accessed June 08, 2020.

E. Black and R. Sutton. The influence of oceanic conditions on the hot european summer of 2003. *Climate dynamics*, 28(1):53–66, 2007.

E. Black, M. Blackburn, G. Harrison, B. Hoskins, and J. Methven. Factors contributing to the summer 2003 european heatwave. *Weather*, 59(8):217–223, 2004.

G. Ceccherini, S. Russo, I. Ameztoy, A. Marchese, and C. Carmona-Moreno. Heat waves in africa 1981âĂŞ2015, observations and reanalysis. *Natural Hazards and Earth System Sciences*, 17: 115–125, 01 2017. doi:10.5194/nhess-17-115-2017.

C. Climate Change Service. Dry and warm spring and summer, 2018. URL https://climate.copernicus.eu/dry-and-warm-spring-and-summer. Last accessed 06 June 2020.

M. Collins, R. Knutti, J. Arblaster, J. Dufresne, T. Fichefet, P. Friedlingstein, X. Gao, W. Gutowski, and T. Johns. 550 krinner. *G., Shongwe, M., Tebaldi, C., Weaver, AJ and Wehner, M.: Long-term Climate Change: Projections, Commitments and Irreversibility, Clim. Chang*, pages 1029–1136, 2013.

Copernicus. Era5 hourly data on single levels from 1979 to present, 2018. URL https://cds.climate.copernicus.eu/cdsapp#!/dataset/reanalysis-era5-single-levels?tab=overview. Last accessed 15 June 2020.

L. Dauphin and J. Stevens. Scarcely seen scandinavian fires, 2018. URL https://earthobservatory.nasa.gov/images/92454/scarcely-seen-scandinavian-fires. Last accessed 14 June 2020.

P. A. Dirmeyer. The terrestrial segment of soil moisture–climate coupling. *Geophysical Research Letters*, 38(16), 2011.

P. A. Dirmeyer, G. Balsamo, E. Blyth, R. Morrison, and H. Cooper. Land-atmosphere interactions exacerbated the drought and heatwave over northern europe during summer 2018. 2020.

F. J. Doblas-Reyes, M. Casado, and M. Pastor. Sensitivity of the northern hemisphere blocking frequency to the detection index. *Journal of Geophysical Research: Atmospheres*, 107(D2): ACL–6, 2002.

W. Dorigo, W. Wagner, C. Albergel, F. Albrecht, G. Balsamo, L. Brocca, D. Chung, M. Ertl, M. Forkel, A. Gruber, et al. Esa cci soil moisture for improved earth system understanding: State-of-the art and future directions. *Remote Sensing of Environment*, 203:185–215, 2017.

i. Encyclopaedia Britannica. Wind, 2020. URL https://www.britannica.com/science/wind. Last accessed June 08, 2020.

T. Fent. Department of economic and social affairs, population division, united nations expert group meeting on social and economic implications of changing population age structures. *European Journal of Population/Revue européenne de Démographie*, 24(4):451–452, 2008.

L. Feudale and J. Shukla. Influence of sea surface temperature on the european heat wave of 2003 summer. part i: an observational study. *Climate dynamics*, 36(9-10):1691–1703, 2011.

C. Gao, H. Chen, G. Li, H. Ma, X. Li, S. Long, B. Xu, X. Li, X. Zeng, H. Yan, et al. Land–atmosphere interaction over the indo-china peninsula during spring and its effect on the following summer climate over the yangtze river basin. *Climate Dynamics*, 53(9-10):6181–6198, 2019.

Geography. How do migrating anticyclones form and affect north america?, n.d. URL https://geography.name/how-do-migrating-anticyclones-form-and-affect-north-america/. Last accessed June 08, 2020.

E. Gilleland. hwmid, n.d. URL https://www.rdocumentation.org/packages/extRemes/versions/2.0-11/topics/hwmid. Last accessed 15 June 2020.

D. Habeeb, J. Vargo, and B. Stone. Rising heat wave trends in large us cities. *Natural Hazards*, 76(3):1651–1665, 2015. doi:https://doi.org/10.1007/s11069-014-1563-z.

E. Jamei and N. Tapper. Wsud and urban heat island effect mitigation. In *Approaches to Water Sensitive Urban Design*, pages 381–407. Elsevier, 2019.

W. Kirch, B. Menne, and R. Bertollini. *Extreme Weather Events*. 2005.

M. Matsueda. Predictability of euro-russian blocking in summer of 2010. *Geophysical Research Letters*, 38(6), 2011.

G. A. Meehl and C. Tebaldi. More intense, more frequent, and longer lasting heat waves in the 21st century. *Science*, 305(5686):994–997, 2004.

D. G. Miralles, A. J. Teuling, C. C. Van Heerwaarden, and J. V.-G. De Arellano. Mega-heatwave temperatures due to combined soil desiccation and atmospheric heat accumulation. *Nature geoscience*, 7(5):345–349, 2014.

M. Mukaka. Statistics corner: A guide to appropriate use of correlation coefficient in medical research malawi medical journal. 2012.

U. Nations. 2018 revision of world urbanization prospects, 2018. URL `https://www.un.org/development/desa/publications/2018-revision-of-world-urbanization-prospects.html`. Last accessed 15 June 2020.

S. E. Perkins and L. V. Alexander. On the measurement of heat waves. *Journal of Climate*, 26 (13):4500–4517, 2013.

T. Peterson, C. Folland, G. Gruza, W. Hogg, A. Mokssit, and N. Plummer. *Report on the activities of the working group on climate change detection and related rapporteurs*. World Meteorological Organization Geneva, 2001.

A. Richling. 2d-blocking, 2016. URL `https://freva.met.fu-berlin.de/about/blocking_2d/`. Last accessed 15 June 2020.

H. Ritchie and M. Roser. Urbanization, 2018. URL `https://ourworldindata.org/urbanization?fbclid=IwAR00NmLnpOjosK1Sl6jGjnANzTCSrG-QVtNiKjOcB1fDy_SoaOHYDfe-tLk`. Last accessed 15 June 2020.

J.-M. Robine, S. L. K. Cheung, S. Le Roy, H. Van Oyen, C. Griffiths, J.-P. Michel, and F. R. Herrmann. Death toll exceeded 70,000 in europe during the summer of 2003. *Comptes rendus biologies*, 331(2):171–178, 2008.

S. Russo, A. Dosio, R. G. Graversen, J. Sillmann, H. Carrao, M. B. Dunbar, A. Singleton, P. Montagna, P. Barbola, and J. V. Vogt. Magnitude of extreme heat waves in present climate and their projection in a warming world. *Journal of Geophysical Research: Atmospheres*, 119 (22):12–500, 2014.

S. Russo, J. Sillmann, and E. M. Fischer. Top ten european heatwaves since 1950 and their occurrence in the coming decades. *Environmental Research Letters*, 10(12):124003, 2015.

S. Russo, J. Sillmann, and A. Sterl. Humid heat waves at different warming levels. *Scientific reports*, 7(1):1–7, 2017.

S. C. Scherrer, M. Croci-Maspoli, C. Schwierz, and C. Appenzeller. Two-dimensional indices of atmospheric blocking and their statistical relationship with winter climate patterns in the euro-atlantic region. *International Journal of Climatology: A Journal of the Royal Meteorological Society*, 26(2):233–249, 2006.

C. Schwierz, M. Croci-Maspoli, and H. Davies. Perspicacious indicators of atmospheric blocking. *Geophysical research letters*, 31(6), 2004.

S. I. Seneviratne, T. Corti, E. L. Davin, M. Hirschi, E. B. Jaeger, I. Lehner, B. Orlowsky, and A. J. Teuling. Investigating soil moisture–climate interactions in a changing climate: A review. *Earth-Science Reviews*, 99(3-4):125–161, 2010.

J. Sillmann, T. Thorarinsdottir, N. Keenlyside, N. Schaller, L. V. Alexander, G. Hegerl, S. I. Seneviratne, R. Vautard, X. Zhang, and F. W. Zwiers. Understanding, modeling and predicting weather and climate extremes: Challenges and opportunities. *Weather and climate extremes*, 18:65–74, 2017.

R. Skaland, H. Colleuille, A. S. H. Andersen, J. Mamen, L. Grinde, H. T. T. Tajet, E. Lundstad, L. F. Sidselrud, K. Tunheim, I. Hanssen-Bauer, et al. Tørkesommeren 2018. Technical report, Technical Report, 2019.

S. Tibaldi and F. Molteni. On the operational predictability of blocking. *Tellus A*, 42(3):343–365, 1990.

W. M. O. WMO. Wmo climatological normals, 2019. URL `http://www.wmo.int/pages/prog/wcp/wcdmp/GCDS_1.php`. Last accessed 07 June 2020.

T. Woollings, D. Barriopedro, J. Methven, S.-W. Son, O. Martius, B. Harvey, J. Sillmann, A. R. Lupo, and S. Seneviratne. Blocking and its response to climate change. *Current climate change reports*, 4(3):287–300, 2018.

P. Zschenderlein, G. Fragkoulidis, A. H. Fink, and V. Wirth. Large-scale rossby wave and synoptic-scale dynamic analyses of the unusually late 2016 heatwave over europe. *Weather*, 73 (9):275–283, 2018.